Title

A genetic switch for male UV-iridescence in an incipient species pair of sulphur butterflies

Authors

Vincent Ficarrotta [a,1], Joseph J. Hanly [a,1], Ling S. Loh [a], Caroline M. Francescutti [a], Anna Ren [a], kalle tunström [b], Christopher W. Wheat [b], Adam H. Porter [c], Brian A. Counterman [d], Arnaud Martin [a,2]

Affiliations

[a] Department of Biological Sciences, The George Washington University, Washington, DC 20052, USA.
[b] Department of Zoology, Stockholm University, Stockholm University, Stockholm, S-10691, Sweden.
[c] Department of Biology, University of Massachusetts Amherst, Amherst, MA 01003, USA.
[d] Department of Biological Sciences, Auburn University, Auburn, AL 36849, USA.
[1] VF and JJH contributed equally to this work.
[2] To whom correspondence should be addressed. Email: arnaud@gwu.edu

Author contributions

V.F., J.J.H., A.H.P, B.A.M. and A.M. conceived the study ; V.F., J.J.H., L.S.L., C.F., A.R., A.H.P., and A.M. performed research; V.F., J.J.H., K.T., C.W.W., A.H.P, B.A.M. analyzed data; V.F., J.J.H. and A.M. wrote the paper with input from all other authors. All authors approved the manuscript before submission.

The authors declare no conflict of interest

Abstract

Mating cues evolve rapidly and can contribute to species formation and maintenance. However, little is known about how sexual signals diverge and how this variation integrates with other barrier loci to shape the genomic landscape of reproductive isolation. Here, we elucidate the genetic basis of UV iridescence, a courtship signal that differentiates the males of *Colias eurytheme* butterflies from a sister species, allowing females to avoid costly heterospecific matings. Anthropogenic range expansion of the two incipient species established a large zone of secondary contact across the eastern US with strong signatures of genomic admixtures spanning all autosomes. In contrast, Z chromosomes are highly differentiated between the two species, supporting a disproportionate role of sex chromosomes in speciation known as the large-X effect. Within this chromosome-wide reproductive barrier, *cis*-regulatory variation of *bric a brac* (*bab*) drives the male UV-iridescence polymorphism between the two species. Bab is expressed in all non-UV scales, and butterflies of either species or sex acquire widespread ectopic iridescence following its CRISPR knock-out, demonstrating that Bab functions as a suppressor of UV-scale differentiation that potentiates mating cue divergence. These results provide new insights into the diversification of sexual signals and the species concept.

Main Text

Premating signals such as pheromones, calls and displays often differ between sexes and species, and by helping animals to tell one another apart, they are integral to the formation of reproductive barriers during speciation itself (1, 2). Mating factors can diverge early in the speciation process due to local adaptation or later due to sexual selection that prevents the generation of unfit hybrids (3). However, how mating cue variation is generated in the first place, and how, in the face of gene flow, it is working with other barrier loci to split lineages, both remain elusive in the empirical literature (4–6).

Previous work on the genetics of hybridization between the sulphur butterflies *Colias eurytheme* and *Colias philodice* highlights their potential for the study of speciation with gene flow. Initially restricted to the Western US, the range of *C. eurytheme* expanded following both the spread of agricultural alfalfa and the reduction in forest cover in the past 200 years into regions once limited to *C. philodice* (7). As a result, the two species occur in secondary sympatry throughout an anthropogenic contact zone that includes the eastern United States and southern Canada. Both pre- and postzygotic reproductive barriers maintain species status in this system. However, heterospecific matings happen at increased frequency in dense populations (8, 9), partly because males can locate newly emerged females incapable of performing mate rejection behaviours [teneral mating (10)]. Hybrid female sterility forms an intrinsic postzygotic barrier that affects one of the two heterospecific crosses: oogenesis fails in female offspring that inherited a *C. eurytheme* W chromosome and a *C. philodice* Z chromosome (11, 12). This incompatibility is sex-linked and implies that to produce fully fertile progeny, *C. eurytheme* females must select males that are homozygous for a conspecific Z chromosome. An iridescent ultraviolet (UV) pattern acts as a visual mating cue in males and accurately displays their Z-chromosome status to females (8, 13) (**Fig. 1A and *Supplementary Material*, Fig. S1**). UV occurs on the dorsal wing surfaces of *C. eurytheme* males only, and this interspecific variation is controlled by the Mendelian *U* locus on the Z chromosome (14): *C. eurytheme* homozygous recessive males are UV-iridescent (*u/u*), advertising two compatible Z chromosomes to *C.eurytheme* females. Incompatible mates such as *C. philodice* males (*U/U*) and heterozygous hybrids (*U/u*) bear the dominant allele and lack UV. Finally, the female preference trait itself is also linked to the Z chromosome (13). This Z-linked inheritence of the genetic incompatibility, mating signal and mating preference support an indicator model of speciation reinforcement where premating and post-zygotic isolation mechanisms are all sex-linked (3, 15, 16). In this study, we examine the genomic footprint of sex-linked reproductive barriers, and fine-map the allelic variation that switches on the male UV signal in *C. eurytheme*.

Results

The Z chromosomes define species barriers in secondary sympatry. To test a putative role of the Z chromosome as a barrier locus, we conducted a genome scan on 22 males from a sympatric population in Maryland, where *C. eurytheme* settled in 1927 (17). We retained 11 UV, orange males and 9 non-UV, yellow males which formed two discrete clusters based on genome-wide SNP clustering by PCA (**Fig. 1C, and *Supplementary Material*, Fig. S2, Table S1**). The Z chromosome showed a drastic increase in genetic differentiation when compared to autosomes (***Supplementary Material*, Figs. S3-4 and Table S2**), with a Z:A ratio of 12:1, the highest sex-chromosome to autosome ratio of F_{ST} reported from a whole genome dataset (6, 18). Heterogeneous landscapes of genomic

differentiation can be explained by local barriers to gene flow or by linked selection in regions of low recombination (6, 19). To parse these two phenomena, we highlighted the top 5% windows of F_{ST} and an above-median recombination rate, thereby identifying three regions — two narrow autosomal F_{ST} peaks, and a 2.5 Mb portion of the Z chromosome (**Fig. 1C, D**). These data show that while only a restricted set of autosomal regions are likely under selection in each population, a large fraction of the Z chromosome is refractory to gene flow in a pattern consistent with a causal role in reproductive isolation.

In addition, nucleotide diversity (π) was depressed on the Z chromosome in both populations and divergence (d_{XY}) was elevated, supporting the inference that the Z chromosome is highly differentiated (***Supplementary Material*, Fig. S3C-D'**). In most scenarios one expects π on the Z chromosome to be 75% of π on the autosomes (20). For *C. eurytheme*, π_Z/π_A was 0.751 ± 0.118, matching this expectation (***Supplementary Material*, Fig. S3E**). However for *C. philodice*, π_Z/π_A was 0.532 ± 0.105, meaning π_Z was lower than expected, which could reflect a skewed sex-ratio, or a recent selective sweep in *C. philodice*.

The male mating signal polymorphism maps to *bab*. The large-Z effect results in extended non-recombining haplotypes in the natural population that prevent association mapping of trait variation (***Supplementary Material*, Fig. S5**). To gain further resolution on the genetic basis of the polymorphic UV signal, we turned to linkage mapping from controlled hybrid crosses. F_2 and backcross (BC) broods showed Mendelian, recessive segregation of the UV state among male offspring (***Supplementary Material*, Fig. S6**). We genotyped 484 recombinant individuals using 2b-RAD sequencing, scored UV among 252 genotyped males, and identified a LOD interval on the Z chromosome (**Fig. 1E and *Supplementary Material*, Fig. S6**). We resequenced individuals with recombination events around the *U* locus and refined a 352 kb zero-recombinant window with 18 annotated genes (**Fig. 1F, G, and *Supplementary Material,* Tables 4-5**). This mapping interval includes the 5' intergenic region, promoter, and first exon of the gene *bric a brac* (*bab*), a salient candidate gene as it encodes a transcriptional repressor of male-limited traits in *Drosophila* such as abdominal pigmentation and sex combs (21–27).

Bab expression is anticorrelated with UV scale cells. To test a role in the regulation of *Colias* male UV, we characterised the expression and developmental functions of *bab* during color scale formation. Butterfly wing scales are macrochaete derivatives that each protrude from a single epidermal cell during pupal development (28). UV scales found in the subfamily Coliadinae are a derived scale type characterised by dense longitudinal ridges; each scale forms a multilayer of chitinous lamellae that selectively reflects UV light by the coherent scattering of incident light (29–32). UV scales are specific to the dorsal wing surface of *C. eurytheme* males, and cover the top of non-UV ground scales (**Fig. 2A, B**). Immunofluorescence at the onset of scale emergence detects Bab expression in the nuclei of all non-UV scale cell precursors (**Fig. 2C, *Supplementary Material*, Fig. S7, Movie S1**) regardless of the scale layer (ground, cover), pigment fate (yellow pterins, black melanin), wing surface, and sex. Remarkably, Bab is expressed in ground scales and is absent in the UV cover scales on the dorsal male wing surface. Thus, Bab is anti-correlated with the UV scale type in *C. eurytheme*: It is consistently expressed in all scale cells fated as non-UV except in the wing cover scales of *C. eurytheme* males. Where it is not expressed in these scales, they develop layered nanostructures specifically capable of UV-iridescent

reflectance. This inactivation in the sexually dichromatic pattern suggests a repressor function, analogous to the expression of Bab in the *Drosophila* abdominal epithelium (21, 23, 27).

CRISPR knock-outs yield ectopic UV-iridescence. To directly test this model, we generated CRISPR-mediated loss-of-function mutations targeting the first exon of the *bab* coding sequence. We collected *C. eurytheme* and *C. philodice* females and microinjected eggs within 7 hrs post-fertilization. G_0 *bab* crispants showed mosaic phenotypes of high penetrance (51 out of 63 surviving adults), with a widespread gain of UV in both males and females of both species, including ventral surfaces, and occasionally on abdominal and leg scales (**Fig. 3, and *Supplementary Material*, Figs. S8-12**). Both pterin and melanin pigment scales, and both cover and ground scales differentiated into UV scales following *bab* KO. Female-specific effects on pigmentation were also noted (***Supplementary Material*, Figs. S8-10**). These loss-of-function assays show that Bab represses the UV identity in all non-UV scale precursors regardless of wing surface, sex, or species. UV iridescence is widespread in the *Colias* genus (32), suggesting that the *C. philodice* absence of UV is due to a secondary loss of Bab repression. The reappearance of UV in *C. philodice* *bab* crispants (an atavism) implies that the underlying network for producing UV scales is still present in this species.

Discussion

Bab is a repressor of male dimorphic traits. Our combined linkage mapping, expression and functional assays of UV iridescence show that *1)* allelic variation of *bab* causes a male-specific mating signal difference between two incipient species; *2)* Bab expression is sexually dimorphic in *C. eurytheme* ; *3)* Bab functions as a repressor of the dimorphic trait. This repression of a male-specific feature is analogous to the expression and function of Bab paralogs in *Drosophila* sex-comb formation, abdominal pigmentation, and gonadal stem cell niches (21–23, 26, 27, 33), with a male-specific repression in the presumptive cells forming the male feature, and loss-of-function resulting in gain or expansion of the male state. Bab is thus a major player in the development of sexually dimorphic features, and might have an ancestral function rooted in the repression of male-specific development in arthropods. It will be critical to study the versatility of its functions comparatively in order to better understand how sexual forms evolve. As knockdowns and knockouts are increasingly amenable in new organisms, testing the repressor nature of Bab should be feasible and may yield a wide range of trait gain or masculinization phenotypes.

bab is a genetic hotspot of sexual phenotypic variation. There is replicated evidence that *cis*-regulatory evolution of *bab* directly causes sexual trait divergence in flies and Lepidoptera (butterflies and moths), making it a genetic hotspot of phenotypic variation (34). In *Drosophila*, linkage mapping studies showed that regulatory alleles of the *bab* locus (*bab1/2* recent paralogs) explain natural variations in dimorphic pigmentation and ovariole number (23, 26, 35). In corn borer moths (*Ostrinia nubilalis*), male response to a polymorphic female pheromone blend is driven by a Z-linked regulatory variation in the first intron of *bab* (36). This same intron is in the *Colias U* locus interval. Thus, the 5’ portion of the lepidopteran *bab* locus drives variation in a male olfactory preference in recently diverged *Ostrinia* species, and in a male visual signal in *Colias*. The *bab* locus is therefore a hotspot for the evolution of reproductive isolation, driving species divergence and maintenance

across Lepidoptera. Factors related to the function, regulation, and genomic location of *bab* may have predisposed it to the tuning of sexually selected traits. First, repressors have drastic effects on cis-regulatory regions and efficiently suppress transcription (37, 38). In this sense, evolving new Bab binding sites in DNA enhancers might be a path of least resistance for optimizing gene expression subtractively, rather than by adding activator binding sites for other selector genes. There is already precedent for the *Drosophila* Bab integrating into a pre-existing network and sculpting sexual dichromatism (27) consistent with this idea. Second, the published expression patterns of Bab show it integrates both spatial and sex-determination inputs (21, 24, 25). Due to a hub-like position in gene regulatory networks, Bab is potentially an input-output gene that facilitates tissue-specific change (39, 40). The large 5′ intergenic and intronic regions of *bab* in *Colias* and *Ostrinia*, or its sub-functionalized duplicates in *Drosophila*, both bode well for a complex cis-regulatory landscape bearing a multitude of enhancers or silencers (41–43), enabling the evolution of precise, tissue-specific changes (44). Last, the location of Bab on the lepidopteran Z chromosome is relevant to the divergence of premating traits under the assumption that sex-chromosomes are more prone to the generation of reproductive isolation than autosomes (20, 45, 46). These possible generative biases will require further investigation among diverged *Drosophila* species, as well as in the *Colias* UV display and *Ostrinia* mate detection systems. Noneless, we speculate that the peculiar molecular function, regulation, and genomic location of Bab may collectively explain its propensity to fine-tune variation in sexual traits.

Extreme Large-X effect in an anthropogenic contact zone. Our genomic scan of differentiation focused on two incipient species that recently reunited due to human activity (alfalfa agriculture). We caught a remarkable signature of a large-Z effect (synonymous with large-X) with widespread admixture across autosomes, and strong differentiation of the entire Z chromosome. This heterogeneous landscape of differentiation is the most extreme identified so far from genome-wide data (18). This supports a role for sex-chromosomes as key drivers of reproductive isolation (20, 45), and even suggests here that the Z chromosome essentially defines species status in north-american sulphur butterflies, while autosomes are exchangable. While linked selection (*syn.* divergence hitchhiking) in regions of low-recombination can sometimes explain such extensive blocks of divergence (6, 19), our linkage map did not indicate this is the case in the *Colias* sympatric pair. The *U* locus in particular overlapped with a large region with above-median recombination, strongly implying that it acts as a genomic barrier to gene flow. Overall, these data establish the anthropogenic contact zones of *Colias* butterflies as a promising system for the study of large-X effects in speciation with gene flow.

Coupling of reproductive barriers. The data in hand suggests the *U* locus variation drives premating isolation by accurately displaying sex chromosome compatibility of courting males to *C. eurytheme* females. In summary, the *Colias* UV mating signal is polymorphic and recessive in areas of secondary contact, with both heterospecific and hybrid males lacking UV because they carry the dominant bab^{U} allele of *C. philodice*. This allele drives uniform expression of Bab, preventing UV scale development with a dominant effect. Conversely, the recessive *C. eurytheme* bab^{u} allele represses expression of Bab in dorsal male cover scales leading to UV fated scales. This Z-linked UV signal allows *C. eurytheme* females to choose Z-compatible mates, thereby pre-zygotically selecting against Z-linked hybrid sterility (3, 8, 9, 11–13). This mechanism strikes us by its sensitivity, given that the recessivity of the trait even allows the rejections of Z-heterozygous males (***Supplementary Material*, Fig. S1**). In

this way, a large-Z effect that couples pre- and post-mating barriers likely drives reinforcement in these butterflies (4, 18), akin to the genetic architectures of speciation in other species (15, 16), and previously conceptualized as an indicator mechanism of speciation reinforcement (3). Further work is needed to decipher other barrier loci on this chromosome. In any case, these findings highlight how a simple genetic switch for a mating cue can influence the origin of species and the maintenance of biodiversity.

Experimental Procedures

Genomic scans of differentiation in sympatric males. Samples originated from a large syntopic population at an alfalfa farm in Buckeystown, MD. Whole-genomes from 24 males were resequenced at 14.3x mean coverage, aligned to the *C. eurytheme* reference genome assembly (47), and used in a population scan analysis pipeline (48).

Linkage map. Interspecific crosses consisting of an F2 and two back-cross broods generated 528 recombinant individuals of known pedigree, sex, and UV phenotype. 2b-RAD sequencing was used to genotype 484 individuals in a HiSeq 4000 SE50 run, using the *Bcg*I enzyme and adapters yielding a 16-fold representation reduction (49). Genotypes were used to build a linkage map as described elsewhere (47). Select individuals were resequenced at a 15x mean coverage to narrow the *U* locus interval.

Bab expression and loss-of-function assays. A custom rabbit polyclonal antibody was generated against the N-terminal 1-365 residues of the *C. eurytheme* Bab protein, and used with a guinea pig anti-Dve (50) for whole-mount immunofluorescence in pupal wings. Heteroduplex mixes of Cas9-NLS and two equimolar sgRNAs (500:125:125 ng/μL) were injected in 1-7 hrs syncytial embryos for targeted mutagenesis of the first exon of *bab.*

CRISPR-mediated KO of *bab*. Two overlapping guide RNA were designed targeting the first exon of bab within the U-locus. Heteroduplex mixes of Cas9:sgRNA1:sgRNA2 (500:125:125 ng/μL) were prepared and microinjected in butterfly syncytial embryos 1-7hrs AEL. Eggs incubated for two days at 28°C then placed on vetch sprouts aged 7-14 days at an average greenhouse temperature of 24°C. Two rounds of injections were successfully performed under these conditions resulting in 51 of 63 adults displaying crispant phenotypes.

UV photography. UV-photography was performed using a full-spectrum converted Lumix G3 camera, mounted with Baader U-Venus filters and UV-transmitting lenses, under the illumination of blacklight bulbs or 365nm LEDs.

Data and Code Availability. Whole-genome sequencing data are available in the Sequence Read Archive (www.ncbi.nlm.nih.gov/sra) under BioProjects PRJNA663300, PRJNA719421, and PRJNA723900. SNP calling, genotyping data, and computer code are available from the Dryad digital repository (48).

Acknowledgements

We thank B. Wang, S. Barao, W. Watt, and R. Canalichio for butterfly rearing, access and expertise, R. Rogers, S. Van Belleghem and P. Rastas for bioinformatics assistance, C. Brantner and C. Day for SEM, M. Matz for 2b-RAD protocols, and M. Perry for the Dve antibody. We also thank core facilities at the GWU, UT Austin, and U. Maryland-Baltimore for generating sequence data. This work was supported by the NSF awards IOS-1755329 and IOS-1656553, and the Swedish Research Council award 2017-04386.

References

1. R. J. Safran, E. S. Scordato, L. B. Symes, R. L. Rodríguez, T. C. Mendelson, Contributions of natural and sexual selection to the evolution of premating reproductive isolation: a research agenda. *Trends in ecology & evolution* **28**, 643–650 (2013).
2. M. R. Servedio, J. W. Boughman, The role of sexual selection in local adaptation and speciation. *Annual Review of Ecology, Evolution, and Systematics* **48**, 85–109 (2017).
3. M. R. Servedio, The evolution of premating isolation: local adaptation and natural and sexual selection against hybrids. *Evolution* **58**, 913–924 (2004).
4. R. K. Butlin, C. M. Smadja, Coupling, reinforcement, and speciation. *The American Naturalist* **191**, 155–172 (2018).
5. D. Ortiz-Barrientos, A. Grealy, P. Nosil, The genetics and ecology of reinforcement. *Annals of the New York Academy of Sciences* **1168**, 156–182 (2009).
6. M. Ravinet, *et al.*, Interpreting the genomic landscape of speciation: a road map for finding barriers to gene flow. *Journal of evolutionary biology* **30**, 1450–1477 (2017).
7. W. Hovanitz, The ecological significance of the color phases of Colias chrysotheme in North America. *Ecology* **25**, 45–60 (1944).
8. R. E. Silberglied, O. R. Taylor, Ultraviolet reflection and its behavioral role in the courtship of the sulfur butterflies Colias eurytheme and C. philodice (Lepidoptera, Pieridae). *Behavioral Ecology and Sociobiology* **3**, 203–243 (1978).
9. O. R. Taylor Jr, Random vs. non-random mating in the sulfur butterflies, Colias eurytheme and Colias philodice (Lepidoptera: Pieridae). *Evolution*, 344–356 (1972).
10. T. J. Thurman, E. Brodie, E. Evans, W. O. McMillan, Facultative pupal mating in Heliconius erato: Implications for mate choice, female preference, and speciation. *Ecology and evolution* **8**, 1882–1889 (2018).
11. J. W. Grula, O. R. Taylor Jr, Some characteristics of hybrids derived from the sulfur butterflies, Colias eurytheme and C. philodice: phenotypic effects of the X-chromosome. *Evolution*, 673–687 (1980).
12. B. Wang, *Introgression and genomic differentiation in sympatric, hybridizing Colias butterflies* (University of Massachusetts Amherst, 2005).
13. J. W. Grula, O. R. Taylor Jr, The effect of X-chromosome inheritance on mate-selection behavior in the sulfur butterflies, Colias eurytheme and C. philodice. *Evolution*, 688–695 (1980).
14. R. E. Silberglied, O. R. Taylor, Ultraviolet differences between the sulphur butterflies, Colias eurytheme and C. philodice, and a possible isolating mechanism. *Nature* **241**, 406–408 (1973).
15. S. A. Sæther, *et al.*, Sex chromosome-linked species recognition and evolution of reproductive isolation in flycatchers. *Science* **318**, 95–97 (2007).
16. D. Ortiz-Barrientos, B. A. Counterman, M. A. Noor, The genetics of speciation by reinforcement. *PLoS Biol* **2**, e416 (2004).
17. A. H. Clark, The butterflies of the District of Columbia and vicinity. *Bulletin of the United States National Museum* (1932).
18. D. C. Presgraves, Evaluating genomic signatures of “the large X-effect” during complex speciation. *Molecular ecology* **27**, 3822–3830 (2018).
19. R. Burri, *et al.*, Linked selection and recombination rate variation drive the evolution of the genomic landscape of differentiation across the speciation continuum of Ficedula flycatchers. *Genome research* **25**, 1656–1665 (2015).
20. M. A. Wilson Sayres, Genetic diversity on the sex chromosomes. *Genome Biology and Evolution* **10**, 1064–1078 (2018).
21. A. Kopp, I. Duncan, S. B. Carroll, Genetic control and evolution of sexually dimorphic characters in Drosophila. *Nature* **408**, 553–559 (2000).

22. J.-L. Couderc, *et al.*, The bric a brac locus consists of two paralogous genes encoding BTB/POZ domain proteins and acts as a homeotic and morphogenetic regulator of imaginal development in Drosophila. *Development* **129**, 2419–2433 (2002).
23. T. M. Williams, *et al.*, The regulation and evolution of a genetic switch controlling sexually dimorphic traits in Drosophila. *Cell* **134**, 610–623 (2008).
24. W. A. Rogers, *et al.*, Recurrent modification of a conserved cis-regulatory element underlies fruit fly pigmentation diversity. *PLoS Genet* **9**, e1003740 (2013).
25. J. R. Salomone, W. A. Rogers, M. Rebeiz, T. M. Williams, The evolution of Bab paralog expression and abdominal pigmentation among Sophophora fruit fly species. *Evolution & Development* **15**, 442–457 (2013).
26. S. De Castro, F. Peronnet, J.-F. Gilles, E. Mouchel-Vielh, J.-M. Gibert, bric à brac (bab), a central player in the gene regulatory network that mediates thermal plasticity of pigmentation in Drosophila melanogaster. *PLoS genetics* **14**, e1007573 (2018).
27. M. J. Roeske, E. M. Camino, S. Grover, M. Rebeiz, T. M. Williams, Cis-regulatory evolution integrated the Bric-à-brac transcription factors into a novel fruit fly gene regulatory network. *Elife* **7**, e32273 (2018).
28. A. Dinwiddie, *et al.*, Dynamics of F-actin prefigure the structure of butterfly wing scales. *Developmental biology* **392**, 404–418 (2014).
29. H. Ghiradella, Development of ultraviolet-reflecting butterfly scales: How to make an interference filter. *Journal of Morphology* **142**, 395–409 (1974).
30. R. L. Rutowski, J. M. Macedonia, N. Morehouse, L. Taylor-Taft, Pterin pigments amplify iridescent ultraviolet signal in males of the orange sulphur butterfly, Colias eurytheme. *Proceedings of the Royal Society B: Biological Sciences* **272**, 2329–2335 (2005).
31. D. J. Kemp, P. Vukusic, R. L. Rutowski, Stress-mediated covariance between nano-structural architecture and ultraviolet butterfly coloration. *Functional Ecology* **20**, 282–289 (2006).
32. D. Stella, Z. Faltỳnek Fric, M. Rindoš, K. Kleisner, P. Pecháček, Distribution of ultraviolet ornaments in Colias butterflies (Lepidoptera: Pieridae). *Environmental entomology* **47**, 1344–1354 (2018).
33. N. Camara, C. Whitworth, A. Dove, M. Van Doren, Doublesex controls specification and maintenance of the gonad stem cell niches in Drosophila. *Development* **146** (2019).
34. A. Martin, V. Orgogozo, The loci of repeated evolution: a catalog of genetic hotspots of phenotypic variation. *Evolution* **67**, 1235–1250 (2013).
35. D. A. Green II, C. G. Extavour, Convergent evolution of a reproductive trait through distinct developmental mechanisms in Drosophila. *Developmental biology* **372**, 120–130 (2012).
36. M. Unbehend, *et al.*, bric à brac controls sex pheromone choice by male European corn borer moths. *Nature Communications* **12**, 2818 (2021).
37. E. P.-B. Noon, F. P. Davis, D. L. Stern, Evolved repression overcomes enhancer robustness. *Developmental cell* **39**, 572–584 (2016).
38. S. S. Gisselbrecht, *et al.*, Transcriptional silencers in drosophila serve a dual role as transcriptional enhancers in alternate cellular contexts. *Molecular cell* **77**, 324–337 (2020).
39. D. L. Stern, V. Orgogozo, Is genetic evolution predictable? *Science* **323**, 746–751 (2009).
40. A. Orteu, C. D. Jiggins, The genomics of coloration provides insights into adaptive evolution. *Nature Reviews Genetics*, 1–15 (2020).
41. L. Baudouin-Gonzalez, *et al.*, Diverse cis-regulatory mechanisms contribute to expression evolution of tandem gene duplicates. *Molecular biology and evolution* **34**, 3132–3147 (2017).
42. G. Kalay, J. Lachowiec, U. Rosas, M. R. Dome, P. Wittkopp, Redundant and cryptic

enhancer activities of the Drosophila yellow gene. *Genetics* **212**, 343–360 (2019).
43. B. Borsari, *et al.*, Intronic enhancers regulate the expression of genes involved in tissue-specific functions and homeostasis. *bioRxiv* (2020).
44. S. B. Carroll, Evo-devo and an expanding evolutionary synthesis: a genetic theory of morphological evolution. *Cell* **134**, 25–36 (2008).
45. M. M. Patten, Selfish X chromosomes and speciation. *Molecular ecology* **27**, 3772–3782 (2018).
46. C. Fraïsse, H. Sachdeva, The rates of introgression and barriers to genetic exchange between hybridizing species: sex chromosomes vs autosomes. *Genetics* **217**, iyaa025 (2021).
47. K. Tunström, *et al.*, A complex interplay between balancing selection and introgression maintains a genus-wide alternative life-history strategy. *bioRxiv*, 2021.05.20.445023 (2021).
48. V. Ficarrotta, *et al.*, Data from: A genetic switch for male UV-iridescence in an incipient species pair of sulphur butterflies (2021). *Available on the DRYAD repository*: DOI:10.5061/dryad.4b8gthtcc
49. S. Wang, E. Meyer, J. K. McKay, M. V. Matz, 2b-RAD: a simple and flexible method for genome-wide genotyping. *Nature methods* **9**, 808–810 (2012).
50. M. Perry, *et al.*, Expanded color vision in butterflies: molecular logic behind three way stochastic choices. *Nature* **535**, 280 (2016).

Main Figures

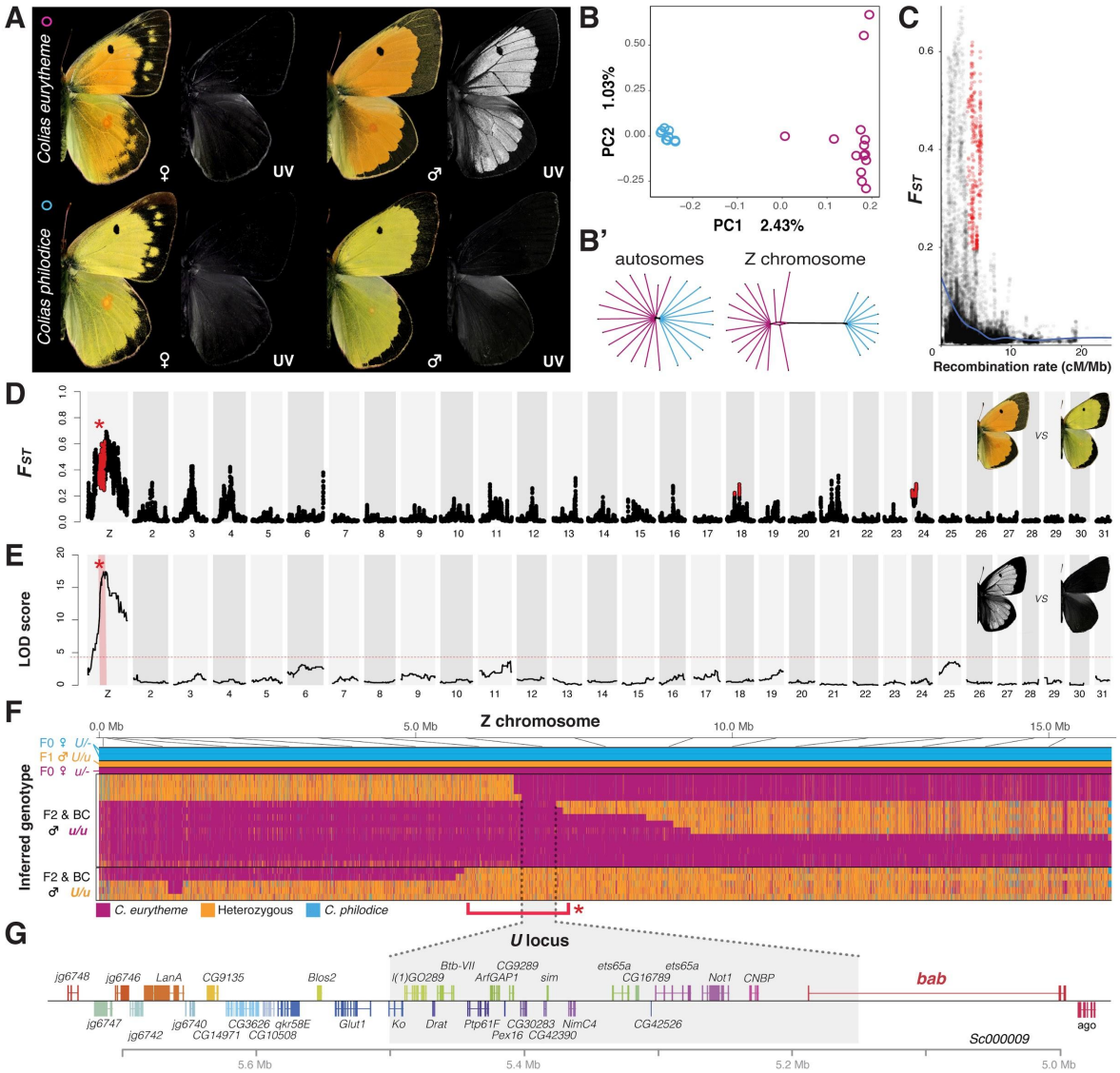

Fig. 1. Large-Z architecture of species differentiation includes the *U* locus candidate gene *bab*. (**A**) UV-iridescence differentiates males from two incipient species. (**B**) PCA and (**B'**) distance-based phylogenetic network of 22 male whole-genome SNPs from the admixed Maryland population. (**C-D**) F_{ST} values for *C. philodice* vs *C. eurytheme* plotted against recombination rate (**C**), and Manhattan plot (**D**). Red indicates windows with above-median recombination rate and in the 95th percentile of F_{ST}, including on the Z chromosome (asterisk). (**E**) QTL analysis of presence/absence of UV in 252 male offspring from F2 and Backcrosses. (**F**) Genotype plot for the whole Z chromosome with resequencing data from 23 individuals. Each row is an individual, and each column is a color-coded SNP. (**G**) Annotation of the *U* locus zero-recombinant interval (box) and surrounding region.

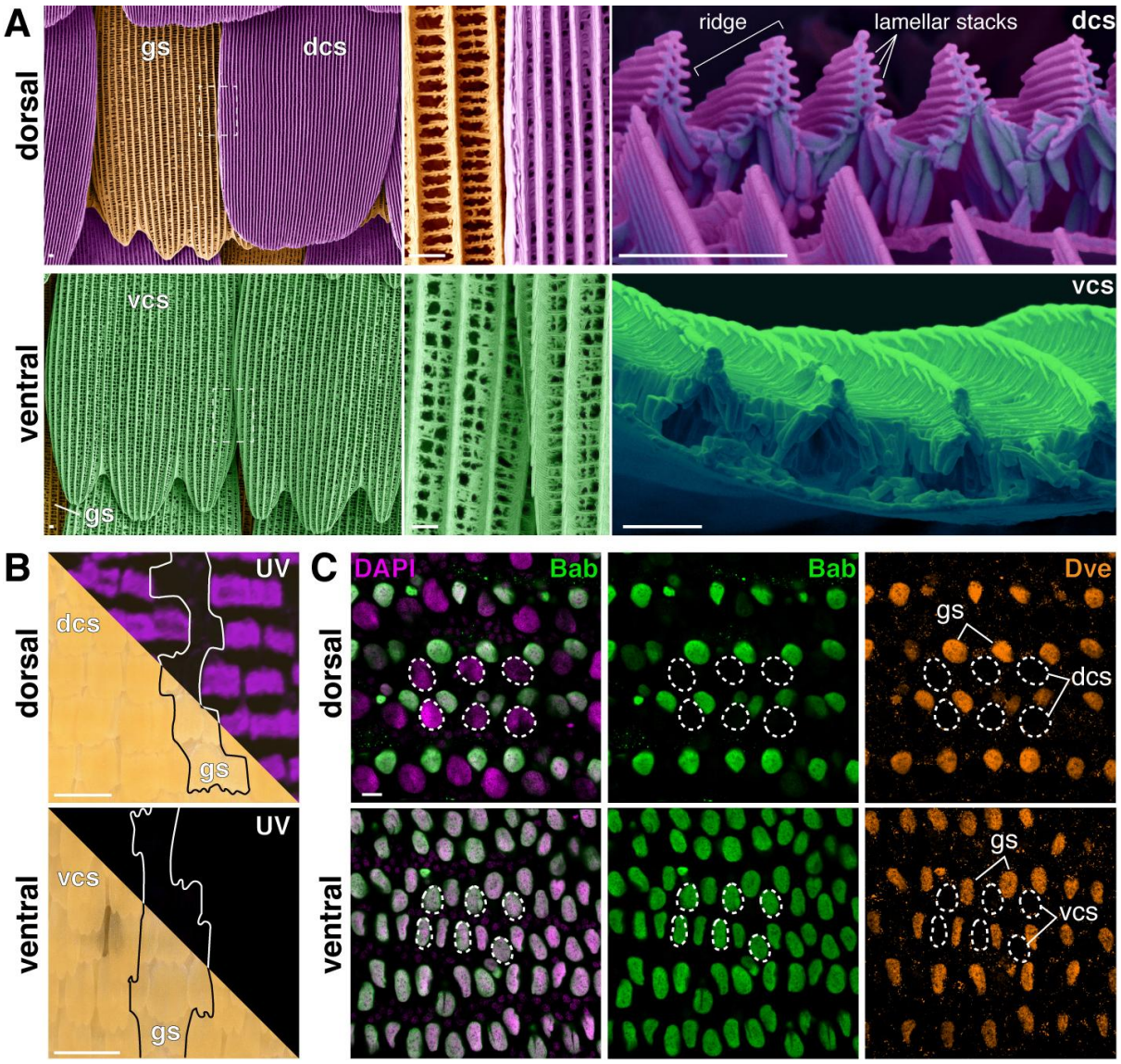

Fig. 2. Bab anticorrelates with UV scale precursors in *C. eurytheme* male wings. (**A**) Pseudo-colored SEMs highlighting the ultrastructural differentiation of the UV+ dorsal cover scales (dcv, magenta), relative to ground scales (gs, orange), and ventral cover scales (vcs, green). (**B**) Microphotographs of adult *C. eurytheme* male wing surfaces in the visible and UV ranges. Line: damaged areas exposing UV-negative ground scales. (**C**) Immunofluorescent detection of Bab (green) in all UV-negative precursors at 46% pupal development. Magenta: DAPI (nuclei) ; orange: Dve ; circles: cover scale nuclei. Scale bars: A = 2 µm ; B = 100 µm ; C = 10 µm.

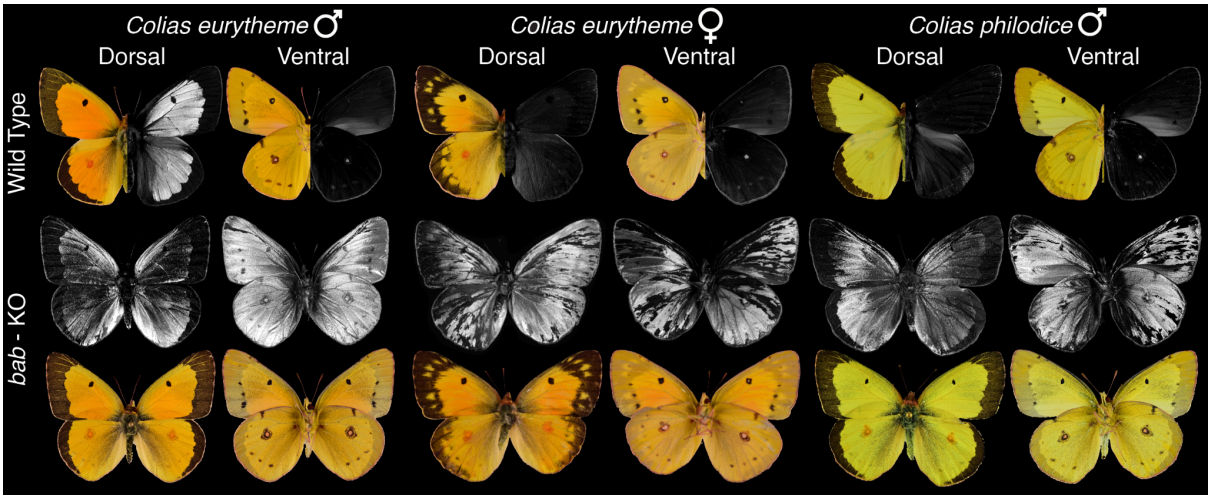

Fig. 3. Bab represses UV scale fate. G_0 phenotypes resulting from CRISPR mosaic KOs targeting the first exon of *bab*. Gain of UV-iridescence was observed across both species and both sexes, including ventral wing surfaces. See **Figs. S11-S12** for additional details.

Supplementary Experimental Procedures

Genomic scans of differentiation in sympatric males

Genome resequencing. We collected and resequenced 24 males (***Supplementary Material*, Table S1**) from a syntopic population found in organic alfalfa fields (Hedgeapple Farm) in Buckeystown, MD. DNA was extracted from thoracic tissues using the Qiagen DNeasy Blood & Tissue Kit, RNAse-treated, and used to prepare a multiplexed sequencing library with the TruSeq PCR-free DNA protocol. The resulting library was sequenced in a first test run using an Illumina NextSeq500 Pair-End 2x75 bp run, and then reloaded in a second Illumina NextSeq500 Pair-End 2x150 bp run, yielding a total of 14.3x coverage per individual on average. Sequencing reads are accessible in the NCBI SRA under the project accession number PRJNA663300.

Alignment, genotyping, and genome-wide analyses. Reads were aligned to the *C. eurytheme* reference genome, derived from a California individual (47). Samples were aligned with BWA-MEM using default parameters (Li, 2013), and variants called using GATK v4.1 with tools HaplotypeCaller and GenotypeGVCFs using default parameters (51). Variant sites were accepted if they were biallelic and the quality (QUAL) value was ≥30. SNPs were phased with Beagle 4.1 (52). Phased SNP variants were used to perform principal component analysis (PCA) using the Eigensoft module SmartPCA (53), and dendrograms were computed using code by Simon H Martin (54) and visualised with SplitsTree (55).

As *C. eurytheme* and *C. philodice* are known to hybridize when found in sympatry at high densities, we sought to determine if any of our sequenced samples were recent hybrids. The PCA showed two main clusters, one containing all *C. eurytheme* and the other containing most *C. philodice*, with clear separation between species along PC1 (***Supplementary Material*, Fig. S2A**). Two samples (numbered *03*, phenotypically identified as *C. philodice,* and *04*, phenotypically identified as *C. eurytheme*), formed a separate cluster. Distance matrix dendrograms grouped these two individuals with the *C. eurytheme* clade, with each other as the closest relative. We determined that these individuals are likely recent hybrids and therefore excluded them from genomic analyses. We re-analysed the data with the likely hybrids removed , and retrieved two clusters with strong separation along PC1. When looking at all genomic data, two *C. eurytheme* individuals were separated on PC2, but were nested within the rest of the *C. eurytheme* individuals on PC1 and in the distance matrix dendrograms (***Supplementary Material*, Fig. S2B**). Likewise, when computing a PCA for just the Z chromosome, two clusters formed with clear separation on PC1, but one individual (numbered 26) was separated by PC2 (***Supplementary Material*, Fig. S2C**). For the rest of the analyses herein, the two sample clusters were used to define each population.

Genome scan using population genetic statistics. We computed population genetic statistics in windows of 100 kb with a sliding overlap of 10 kb (48, 54). Mean genome-wide divergence indicated by fixation index (F_{ST}) between species is low, with peaks of high divergence on autosomes (***Supplementary Material*, Fig. S3A, B**). The Z chromosome shows considerably higher mean divergence than autosomes, consistent reduced gene flow of the

sex chromosome caused by hybrid inviability, and is also consistent with the observation that wing patterning traits in *Colias* are clustered on the Z chromosome (12).

Recombination rate in interspecific crosses. Genome-wide recombination rate was computed from the linkage map using the R package MareyMap (56) using a loess smooth with a span of 1 Mb and a degree of 1. A cM/Mb value was extracted for 100 kb intervals along the entire genome (***Supplementary Material,* Fig. S3F**).

Linkage mapping of UV variation in males

Mapping crosses. Interspecific crosses consisting of an F2 and two back-cross broods (named broods 75, 49, and 79 respectively) were reared in the laboratory of Adam Porter in 2000 and described in a previous publication (12). Briefly, the offspring of wild-caught females from the vicinity of Amherst and Sunderland, MA were reared in the laboratory for species assignment, and used for controlled crosses over two generations where all brood pedigrees and phenotypes were recorded. UV-iridescence showed binary presence-absence and Mendelian segregation ratios that confirmed the recessive and sex-linked inheritance the *U* locus (***Supplementary Material*, Fig. S5**). Crossing-over is absent from lepidopteran females but recombination is expected in the hybrid F1 fathers (ZZ) of those three crosses, which are thus informative for the mapping of the male-expressed and Z-linked *U* locus. A total of 528 adult F2 and BC butterflies were frozen at -80°C after emergence until further analysis.

DNA extraction. Frozen adult specimens from the mapping broods were each given an identifier, and sequentially processed for genotyping and phenotyping. Wings of each individual were removed and dispatched into glassine envelopes, the dorsal half of the thorax was excised and transferred to the well of a 96 Collection Microtube Rack (Qiagen, USA) with a 3.5mm stainless steel bead, and the rest of the body was stored in an individual tube for frozen storage. To prevent cross-contamination of DNA samples, each individual was processed on a new aluminium foil surface and tools were cleaned in 5% bleach, rinsed in distilled H_2O, and dried with EtOH 70% between samples. Thoracic tissue samples were mixed with 400 µl of BeadBashing Buffer (Zymo Research, USA), and homogenised in the collection racks on a MM400 mixer mill (Retsch, Germany) fitted with a TissueLyser 2 x 96 Adapter Set (Qiagen, USA) for 4 min at 30 Hz. Following centrifugation, the supernatant from those homogenates was DNA-extracted while maintaining a 96-well microplate format using the Quick-DNA 96 kit (Zymo Research, USA), eluted in 50 µL of DNA Elution Buffer, and quantified with a Qubit dsDNA High-Sensitivity kit.

Preparation of the 2b-RAD sequencing library. The mapping broods resulted in 497 DNA samples spread across six 96-well plates (48). We used 2b-RAD genotyping with a multiplexed strategy to pool all the samples into a single sequencing library (49, 57). 2b-RAD sequencing uses Type IIb restriction enzymes that cleave DNA on both sides of their targets. We used the *Bcg*I enzyme to generate 34 bp fragments flanked by barcoded sequencing adapters (***Supplementary Material*, Table S3**). Adapters terminated on each side end with NG-3' instead of NN-3', resulting in a 16-fold reduction in the representation of all restriction sites. Samples were dispatched in new microplates with 200 ng of DNA per sample (25 µL,

normalised at 8 ng/μL), digested with *Bcg*I, heat inactivated, and purified with the ZR-96 Oligo Clean & Concentrator kit (Zymo Research, USA) in a final elution volume of 12 μL. The purified restricted DNA was then ligated with the generic 5' adapter (*5ILL-NG*) and with a different 3' adapter (*3illBC1-12*) in each column, before heat inactivation and pooling of the 12 plate columns into a single strip of 8 rows. This product was then PCR amplified for 14 cycles with standard Illumina adapters (IC1-P5, IC2-P7, and NEB Universal PCR primer) as well as one of 48 unique barcoded adapters (*NEBNext Multiplex Oligos Index Primers Sets 1-3*), yielding a visible band of about 170 bp on an agarose gel. Those products were quantified by fluorometry and pooled into a single library. A sequencing facility purified the target product of 170 bp using a BluePippin instrument equipped with 3% Agarose DNA cassettes (Sage Science, USA), quality checked, mixed with a 20% *PhiX* phage library, and sequenced using a Illumina HiSeq 4000 SE50 run.

Linkage mapping of the U locus. The linkage map was built in LepMap3 as previously described (47). Data were imported to R/qtl as a four-way cross (48, 58). First, we performed a QTL analysis with the male samples, treating the presence or absence of UV as a binary trait and performing 1000 permutations to determine a confidence threshold. A strong QTL peak was identified on the Z chromosome, with an extended LOD interval. As the trait is Mendelian, we then looked for regions on the Z chromosome that showed an inheritance pattern that was completely consistent with phenotype (zero recombinant window), and identified a number of individuals with recombinations around marker 41 (***Supplementary Material*, Fig. S6**).

Resequencing of recombinant individuals. To identify the precise breakpoints in these recombinant individuals, we resequenced their undigested genomes at 15x mean coverage using an Illumina NovaSeq S1 2x150bp run, along with three brood grandmothers and an F1 male (***Supplementary Material*, Table S4**). Raw reads were deposited in the SRA under the BioProject PRJNA719421. These samples were aligned, variant-called and phased as above. We filtered Z Chromosome SNPs for sites where both the *C. philodice* and *C. eurytheme* grandmothers had alternate alleles and the F1 male was heterozygote. The data for the Z chromosome was visualised using *genotype_plot* (48, 59, 60), and breakpoints manually identified (***Supplementary Material*, Fig. S4**). This visualisation includes the individuals from Buckeystown, MD; note that individual 26, which in the Z chromosome PCA was separated on PC2 from the other *C. eurytheme* (***Supplementary Material*, Fig. S2C**), appears to contain a large heterozygous block of *C. philodice* haplotype on the 3' end of the Z chromosome.

We refined the *U* locus (**Fig. 1E**) to the interval between the breakpoints in individuals *00-79-099* and *00-49-013*, which runs between positions *Sc000009*: 5173306-5525979. There are 18 annotated transcripts within or overlapping this interval in the *C. eurytheme* GFF (***Supplementary Material*, Table S5**) including the first exon and part of the first intron of the gene *bab*.

Protein coding alignment of Bab. Variants in the protein coding sequence of *bab* were extracted for each resequenced individuals (***Supplementary Material*, Tables S1, 4**), converted to FASTA format using *bcftools*, and aligned with *MAFFT* in Geneious. No amino acid or nucleotide variants were fixed between UV-iridescent and non-iridescent males,

though some polymorphism exists within these two populations. Nucleotide and amino acid alignments are available on DRYAD (48). There are no coding variants in the first exon, the only coding exon of *bab* situated within the boundaries of the *U* locus, implying that the *bab* variation responsible for the UV interspecific polymorphism is of *cis*-regulatory nature.

Expression and loss-of-function assays

Antibodies. The production of the custom rabbit anti-Bab polyclonal antibody was outsourced to a manufacturer (GenScript Biotech, NJ). A sequence encoding His-tagged amino-acid residues 1-365 from the *C. eurytheme* annotated protein was cloned in the *pET-30a* plasmid, and purified from bacteria with a His-tag before immunisation of two rabbits, from which polyclonal sera were affinity purified before use. The guinea pig anti-Dve antibody was a kind gift from Michael Perry (UC San Diego), and recognises a butterfly homolog of Defective proventriculus (50). Secondary antibodies used include conjugated AlexaFluor647 anti-Rabbit IgG (Life Technologies, CA) at 1:100 dilution, and conjugated AlexaFluor555 goat anti-guinea pig IgG (Abcam, UK) at 1:400 dilution.

Immunostainings. Colias spp. larvae were reared on 1-3 week old sprouts of Lana woolypod vetch (*Vicia villosa*) grown on hemp mats, and monitored for pupation throughout the day. Pupal developmental stages were temperature-dependent, with average adult emergence of 192 h APF (hours after pupa formation) at 24 °C and 144 h APF at 28 °C. Pupae were dissected at stages spanning 30-45% developmental time in phosphate buffer saline (PBS), fixed for 12 m at room temperature in formaldehyde 4% (PBS, EGTA 2mM), washed in PBS 0.1% Triton X-100 (PT 0.1%), blocked with PT 0.1% with 0.5% bovine serum albumin for a minimum of 30 m, incubated with primary antibodies overnight at 4 °C (anti-Bab, 1:100 dilution ; anti-Dve, 1:400 dilution), washed, incubated with secondary antibodies at room temperature for 2 h, washed, incubated in 50% glycerol, PBS, 1 µg/ml DAPI for nuclear counterstaining, mounted on glass slides with 70% glycerol under a #1.5 thickness coverslip, and sealed with nail varnish before imaging.

Confocal imaging. Stacked acquisition were acquired using an Olympus FV1200 inverted laser scanning confocal microscope mounted with a 60x Apochromat oil-immersion objective (PLANAPO, 1.42NA), and equipped with a laser line for excitation at 405 nm (DAPI), 488 nm (Phalloidin-OregonGreen), 555 nm (anti-Bab / AlexaFluor555) and 647 nm (Dve / AlexaFluor647). Z-stacks were visualised in 2D using FIJI/ImageJ and in 3D with Imaris 3D/4D visualization software (Bitplane AG, Switzerland).

CRISPR-Cas9 mediated knockouts. Two unique sgRNA targets were designed in the first exon of *bab* in a region void of SNPs (*Ceu_bab_sgRNA1* target: 5'-ACTGTTGGGGCGAGCCGGG-3' ; *Ceu_bab_sgRNA2* target: 5'-CGGCGGGCCCGGCTCCTCG-3'). Heteroduplex mixes of Cas9:sgRNA1:sgRNA2 (500:125:125 ng/µL) were prepared and microinjected in butterfly syncytial embryos as previously described (61). Continuous captive rearing of *C. eurytheme* and *C. philodice* is challenged by the sensitivity of the larvae to viral disease (62), and we thus used wild-caught females (Hedgeapple Farm, Buckeystown, MD) to obtain eggs from both species. Females were placed in 28 cm foldable cages with a high density of fresh

alfalfa cuts in water, and under F54T5HO fluorescent tubes. Eggs were surface sterilised in 5% benzalkonium chloride, rinsed, dried, positioned on double-tape, microinjected 1-7 hrs after egg laying, placed in a plastic tupperware with a moist paper towel at constant 28 °C for 24-48 hrs and placed on vetch sprouts aged 7-14 days at an average greenhouse temperature of 24 °C. Trays of 8-21 days old vetch were added as necessary and surviving individuals reached adulthoods in an average of 30 days after egg laying. Larval mortality was high due to viral disease including in uninjected batches. Two rounds of *bab* CRISPR injections were performed : the first round resulted in 50 emerged G_0 adults (997 eggs injected) who all showed mosaic, ectopic gains of UV-iridescence ; the second round resulted in 13 G_0 adults (136 eggs injected) of which 11 showed positive results and 2 appeared wild-type.

Phenotyping and imaging

Photography in the ultraviolet and visible ranges. We combined digitisation in the visible color range and UV-photography to phenotype the wings of the individuals used in this study. For UV imaging, wings and specimens were illuminated by CFL BlackLight 13 Watt T3 Spiral Light Bulbs (General Electric, USA), and photographed using a modified Panasonic/Lumix G3 with full-spectrum UV/VIS/IR conversion purchased from an online retailer (Infraready, UK). For selective imaging of the UV reflectance, this camera was mounted with a custom-modified 75mm UV-transmitting lens (source : eBay user Igoriginal), stopped at f/11, on an Adjustable T-to-M4/3 Mount Lens Adapter, and fitted with a Baader 2'' U-Venus-Filter (Baader Planetarium, Germany), which transmits 80% of light 350 nm but blocks all visible light in the visible range above 400 nm. For UV-microphotography of scales, the same camera was mounted with an Olympus UPLANFL N 10x/0.30NA objective fitted with a Baader 1¼'' U-Venus-Filter. At this higher magnification range, best results were obtained with increased illumination using an U301 365nm Nichia UV LED Flashlight (MTE, China). Pinned specimens were photographed in the visible range using a Nikon D5300 camera mounted with a Micro-Nikkor 105mm f/2.8G lens on a StackShot rail, and focused-stacked using Helicon Remote and Helicon Focus (Helicon Soft, Ukraine). A Keyence VHX-5000 digital microscope was used to generate stitched high-resolution images of wing patterns using a VH-Z00T lens at 50X magnification and a VH-Z100T lens at the 300X magnification. The excised wings of all sequenced specimens were scanned on an Epson Perfection V600 scanner at 6,400 dpi resolution next to a color reference card.

Scanning electron microscopy. For surface imaging of ground and cover scales, regions of interest were excised and mounted on SEM stubs with double-sided carbon tape and sputter coated with 10 nm of gold. Images were acquired on a FEI Teneo LV FEG SEM, using secondary electrons (SE) and an Everhart-Thornley detector (ETD) with a beam energy of 2.00 kV, beam current of 25 pA, and a 5 µs dwell time. Individual images were stitched using the Maps 3.19 software (ThermoFisher Scientific). To document scale ultrastructure, regions of interest were excised and cryo-fractured following previous recommendations (63–65). Excised wing sections were placed target-side down onto a silicon wafer and secured with foam board, glassine, and a binder clip before submersion in liquid nitrogen, and immediately cut with a fresh ceramic-coated microtome blade. After drying, individual cut scales were placed on copper tape using an eyelash tool, such that the cut edges were

approximately parallel to and overhanging the tape edge. The copper tape was bent to 90° and placed on a stub so that the scales' cut edges faced upwards, *i.e.* normal to the stub surface, and secured with additional copper tape. Stubs were sputter coated with a 10 nm layer of gold, and imaged at 5.00 kV / 6.3 pA and a 10 µs dwell time.

Supplementary Material References

51. A. McKenna, *et al.*, The Genome Analysis Toolkit: a MapReduce framework for analyzing next-generation DNA sequencing data. *Genome research* **20**, 1297–1303 (2010).
52. S. R. Browning, B. L. Browning, Rapid and accurate haplotype phasing and missing-data inference for whole-genome association studies by use of localized haplotype clustering. *The American Journal of Human Genetics* **81**, 1084–1097 (2007).
53. A. L. Price, *et al.*, Principal components analysis corrects for stratification in genome-wide association studies. *Nature genetics* **38**, 904–909 (2006).
54. S. H. Martin, *simonhmartin/genomics_general* (2021) (March 11, 2021).
55. D. H. Huson, D. Bryant, Application of phylogenetic networks in evolutionary studies. *Molecular biology and evolution* **23**, 254–267 (2006).
56. C. Rezvoy, D. Charif, L. Guéguen, G. A. Marais, MareyMap: an R-based tool with graphical interface for estimating recombination rates. *Bioinformatics* **23**, 2188–2189 (2007).
57. M. V. Matz, 2bRAD_denovo. *GitHub*.
58. D. Arends, P. Prins, R. C. Jansen, K. W. Broman, R/qtl: high-throughput multiple QTL mapping. *Bioinformatics* **26**, 2990–2992 (2010).
59. J. R. Whiting, Genotype_Plot. *GitHub*.
60. J. R. Whiting, *et al.*, Drainage-structuring of ancestral variation and a common functional pathway shape limited genomic convergence in natural high-and low-predation guppies. *bioRxiv* (2020).
61. A. Martin, N. S. Wolcott, L. A. O'Connell, Bringing immersive science to undergraduate laboratory courses using CRISPR gene knockouts in frogs and butterflies. *Journal of Experimental Biology* **223** (2020).
62. E. A. Steinhaus, Crowding as a possible stress factor in insect disease. *Ecology* **39**, 503–514 (1958).
63. B. R. Wasik, *et al.*, Artificial selection for structural color on butterfly wings and comparison with natural evolution. *Proceedings of the National Academy of Sciences* **111**, 12109–12114 (2014).
64. Y. Matsuoka, A. Monteiro, Melanin pathway genes regulate color and morphology of butterfly wing scales. *Cell reports* **24**, 56–65 (2018).
65. R. C. Thayer, F. I. Allen, N. H. Patel, Structural color in Junonia butterflies evolves by tuning scale lamina thickness. *bioRxiv*, 584532 (2019).
66. S. H. Martin, J. W. Davey, C. Salazar, C. D. Jiggins, Recombination rate variation shapes barriers to introgression across butterfly genomes. *PLOS Biology* **17**, e2006288 (2019).
67. A. Ren, *et al.*, Convergent evolution of broadband reflectors underlies metallic coloration in butterflies. *Frontiers in Ecology and Evolution* **8**, 206 (2020).

Supplementary Material Figures

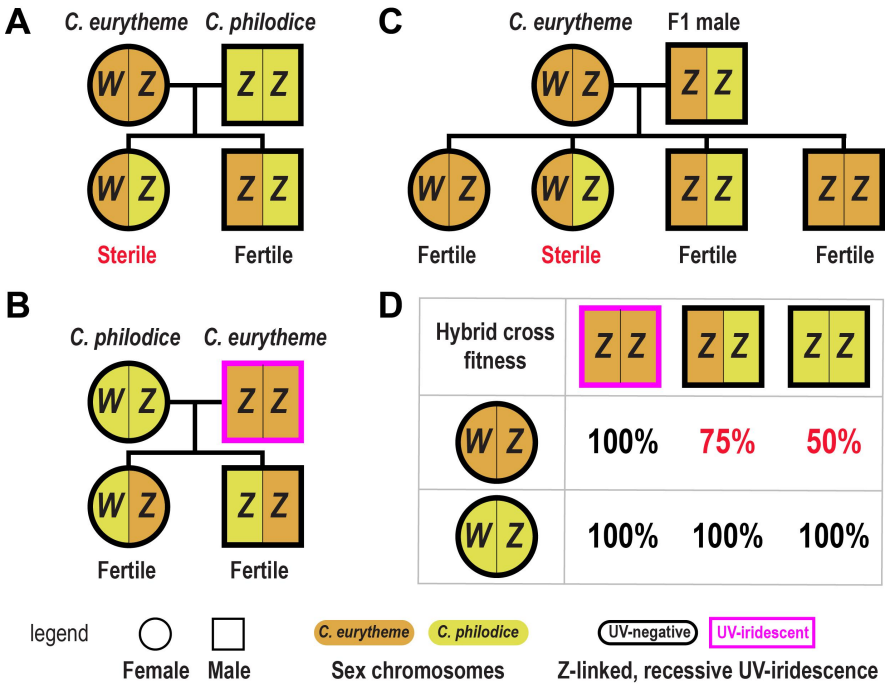

Figure S1. Female hybrid sterility in North American sulphur butterflies. (**A-C**) Data summary from Taylor and Grula (11) illustrating the pattern of Z-linked female hybrid sterility in sympatric *C. eurytheme x philodice*. (**D**) Parental crosses involving a *C. eurytheme* W mother and *C. philodice* Z sperms suffer a reproductive fitness reduction (red), but these incompatibilities can be avoided by assortative mating of *C. eurytheme* females with UV-iridescent males homozygous for the *C. eurytheme* Z chromosome. Sterile females develop normally but undergo ovarian failure, a phenomenon that could arise from incompatibility of the *C. eurytheme* matrilineal elements (W chromosome, mitochondrial genome) with the *C. philodice* Z chromosome during oogenesis, or from a conflict between the *C. philodice* Z and an autosomal *C. eurytheme* incompatibility locus.

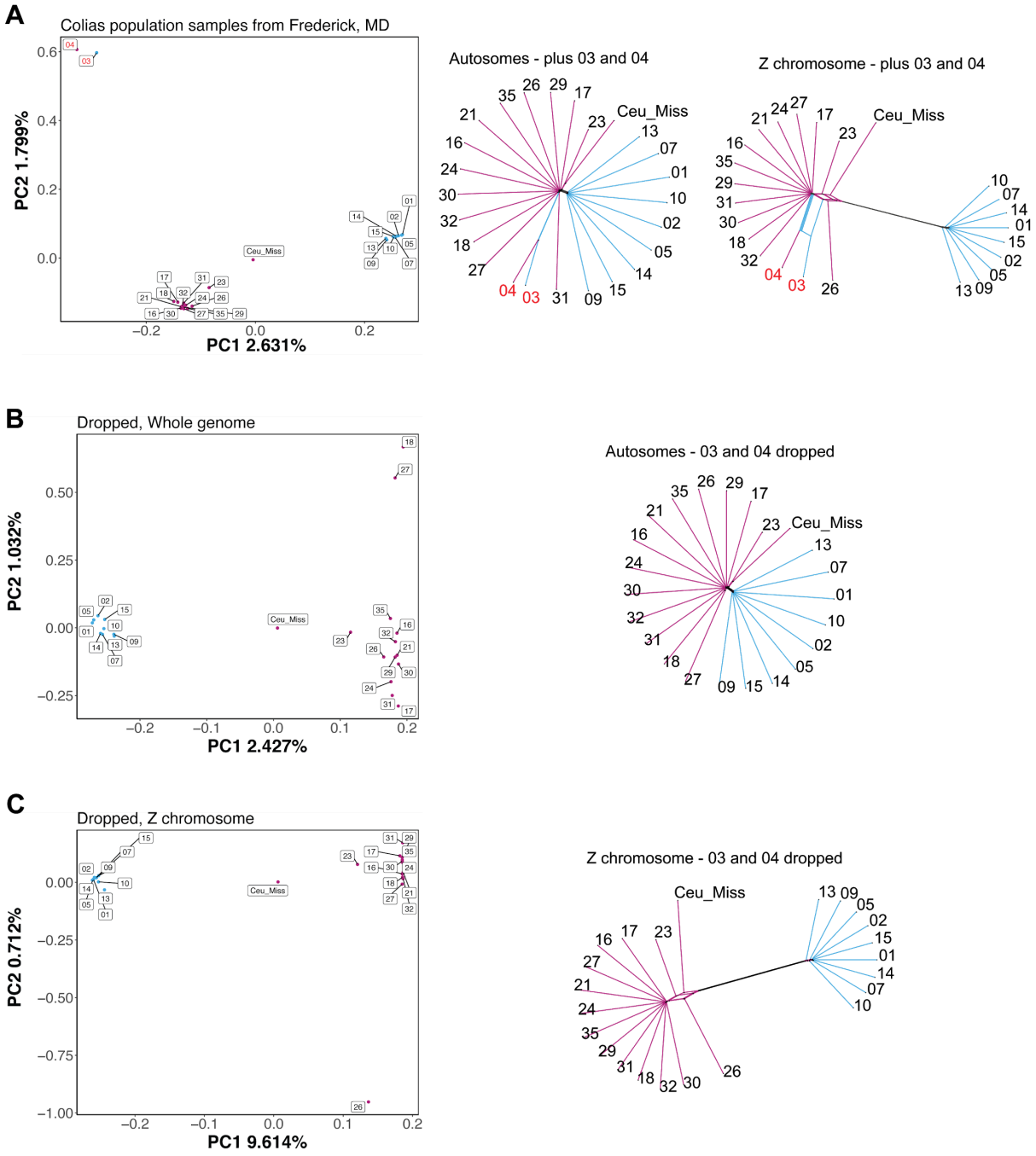

Figure S2. Principal component and phylogenetic network analyses of individuals collected in central Maryland. (**A**) Genome-wide SNP PCA and dendrogram of all males sampled from the admixed Maryland population, plus a *C. eurytheme* male collected in Mississippi. (**B**) Two samples (red) that did not cluster with either species were removed. (**C**) Analysis repeated for just the Z chromosome. Individual genomes were assigned to a *C. eurytheme* (magenta) or *C. philodice* (cyan) cluster in subsequent population scans.

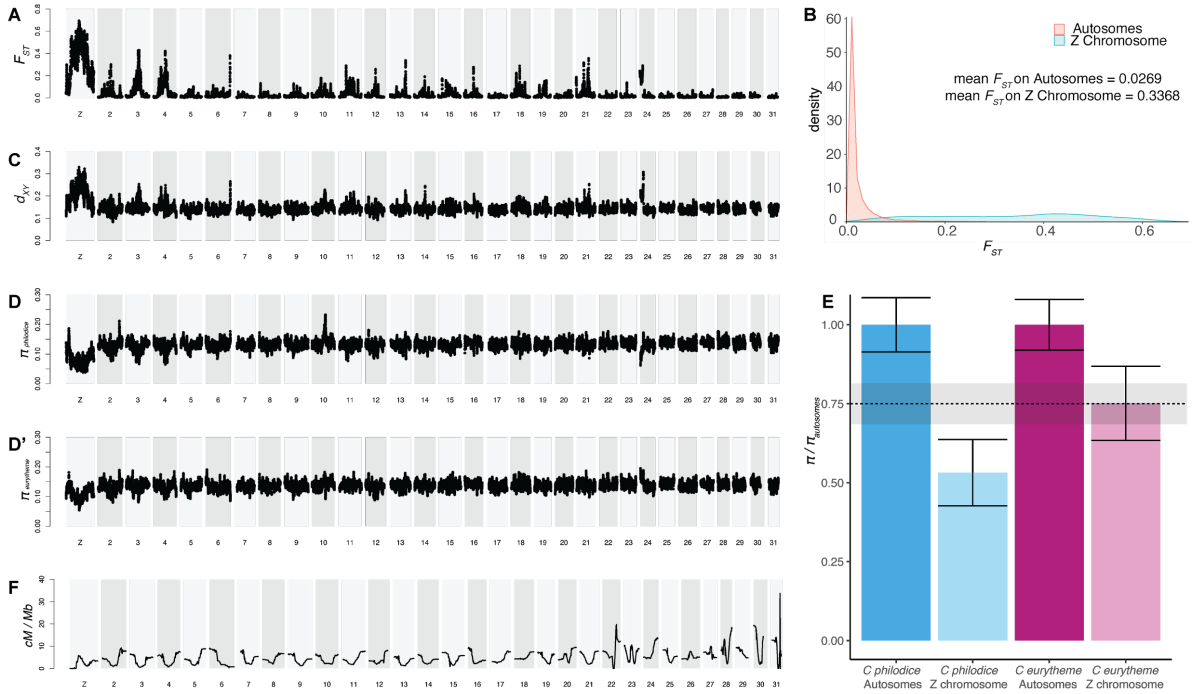

Figure S3. Population statistics for the central Maryland population of *C. philodice* and *C. eurytheme*. (**A-B**) Unadorned F_{ST} Manhattan plot and histogram of F_{ST} on autosomes versus the Z chromosome. (**C**) d_{XY} and (**D-D'**), π statistics. (**E**) π_A/π_A vs π_Z/π_A , with the dotted line and shading representing the expected mean value and confidence interval for the π_Z/π_A ratio around 0.75. (**F**) genome-wide recombination rates derived from the linkage map from the backcross and F2 broods (***Supplementary Material*, Fig. S5**). Ends of chromosomes tend to show higher recombination than centres, and shorter chromosomes were found to have a higher recombination rate than longer ones. This inverse relationship between chromosome size and recombination rate is reminiscent of previous findings in *Heliconius* butterflies (66).

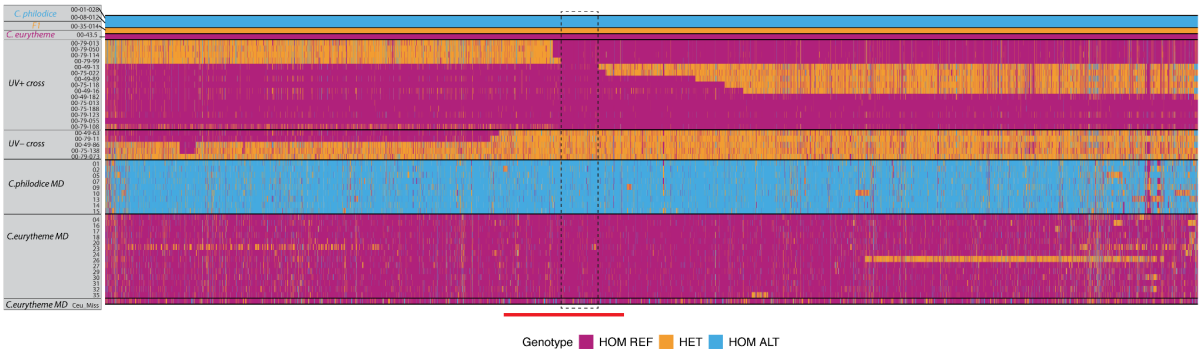

Figure S4. Genotype plot of the Z chromosome for all sequenced samples. A reproduction of **Fig. 1G**, including the samples collected in central Maryland and the *C. eurytheme* individual from Mississippi. The dotted box and red line indicate the same intervals as in **Fig. 1G**. Sample *Ceu26* has a heterozygous haplotype that takes up a large portion of the Z chromosome , and other individuals of both *C. eurytheme* and *C. philodice* carry shorter heterozygous haplotypes. This provides evidence that some limited ongoing sex-chromosome admixture exists in this wild population, permitting some recombination and persistance in the heterozygous state.

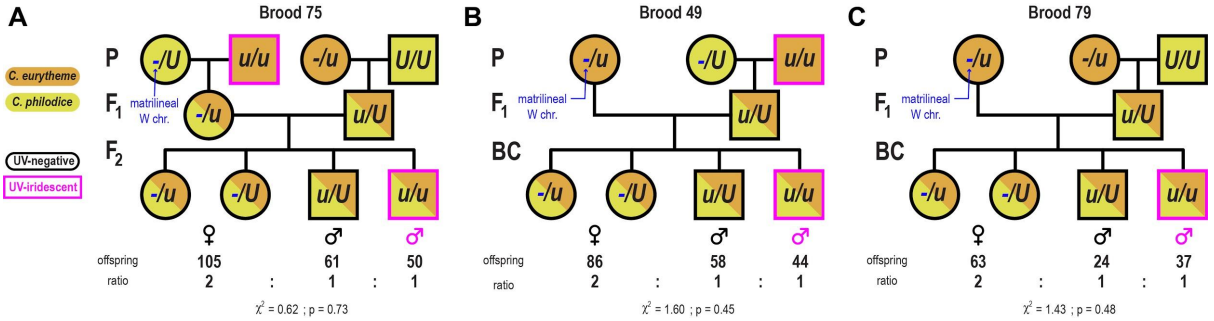

Figure S5. Mapping crosses. The UV trait segregated at the expected 1:1 ratio among the male offspring, in the three crosses that were used for fine mapping the *U* locus. **(A)**, F2 cross. **(B-C)** Backcrosses to *C. eurytheme*, with the second *u* allele inherited from the paternal grandfather (**B**) or paternal grandmother (**C**). Chi-square tests show non-significant deviations from 2:1:1 distributions (females : non-UV males : UV males) that are expected from a Mendelian recessive, sex-linked mode of inheritance of the UV-iridescent state.

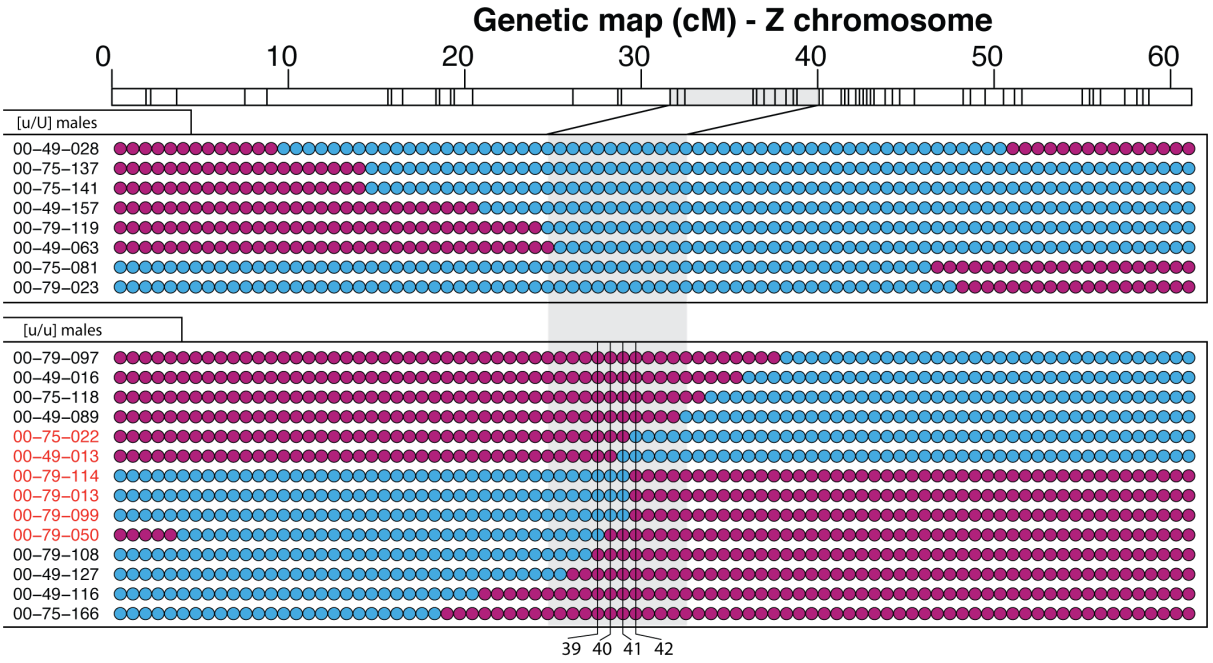

Figure S6. Identification of recombinant individuals in 2b-RAD data. Each row is a recombinant, patrilineal Z chromosome from a male individual, each column is a 2b-RAD marker. All F2 and BC male offspring have a non-recombining matrilineal Z chromosome of *C. eurytheme* ancestry (*i.e.* bearing an *u* allele), due to the nature of the crosses (***Supplementary Material*, Fig. S5**). Colors indicate allelic states across the recombining, patrilineal Z chromosome — magenta : *C. eurytheme* ancestry ; blue : *C. philodice* ancestry. The scale at the top shows the linkage map for the Z chromosome, with the 1.5-LOD support interval for the *U* locus shaded in grey. Red-highlighted individuals had recombination breakpoints between markers 39-42 and were used (along with additional samples) for whole genome resequencing.

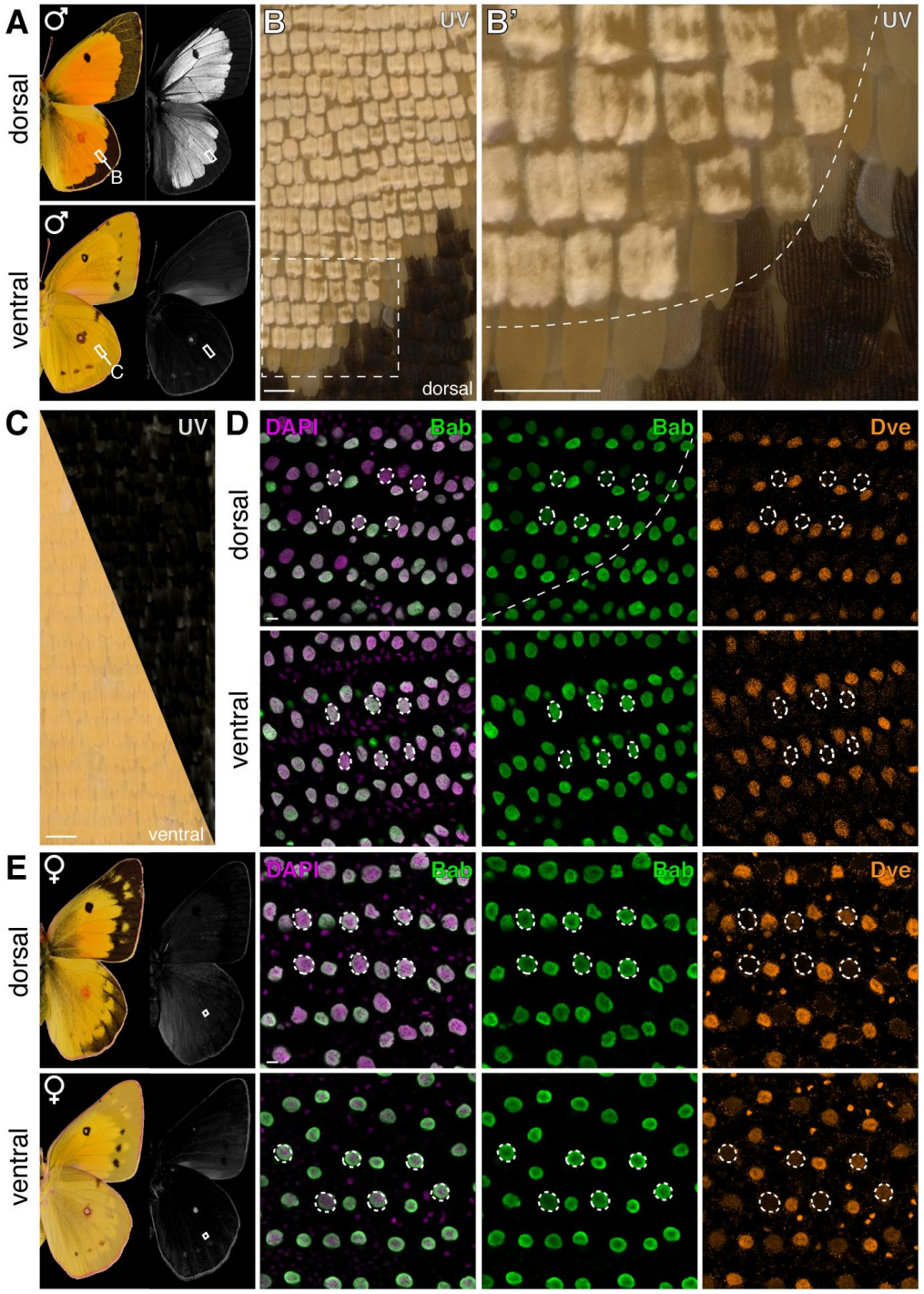

Figure S7. Bab expression is restricted to non-UV scale cell precursors during *C. eurytheme* pupal wings. (**A-C**), UV-photography (white) shows the UV-iridescent cover scales are specific to large orange-yellow areas of the dorsal surface of *C. eurytheme* males. Melanic cover scales, and a fraction of yellow-orange cover scales (*e.g.* in **B-B'** at the interface with the melanic margin) are UV-negative. Ventral discal spots show broad-spectrum metallic reflectance rather than UV-iridescence (67). (**D**) Immunodetection of Bab in a male pupal wing (46% development), in the region shown in (**B'**). Bab is ubiquitous in the UV-negative wing regions. In the dorsal UV-iridescent region, Bab is limited to Dve-positive ground scales, and is repressed in cover scales (circles). (**E**), Ubiquitous expression of Bab and Dve observed in both dorsal and ventral surfaces of a female *C. eurytheme* hindwing (37% development). Scale bars: B-C = 100 µm ; D-E = 10 µm.

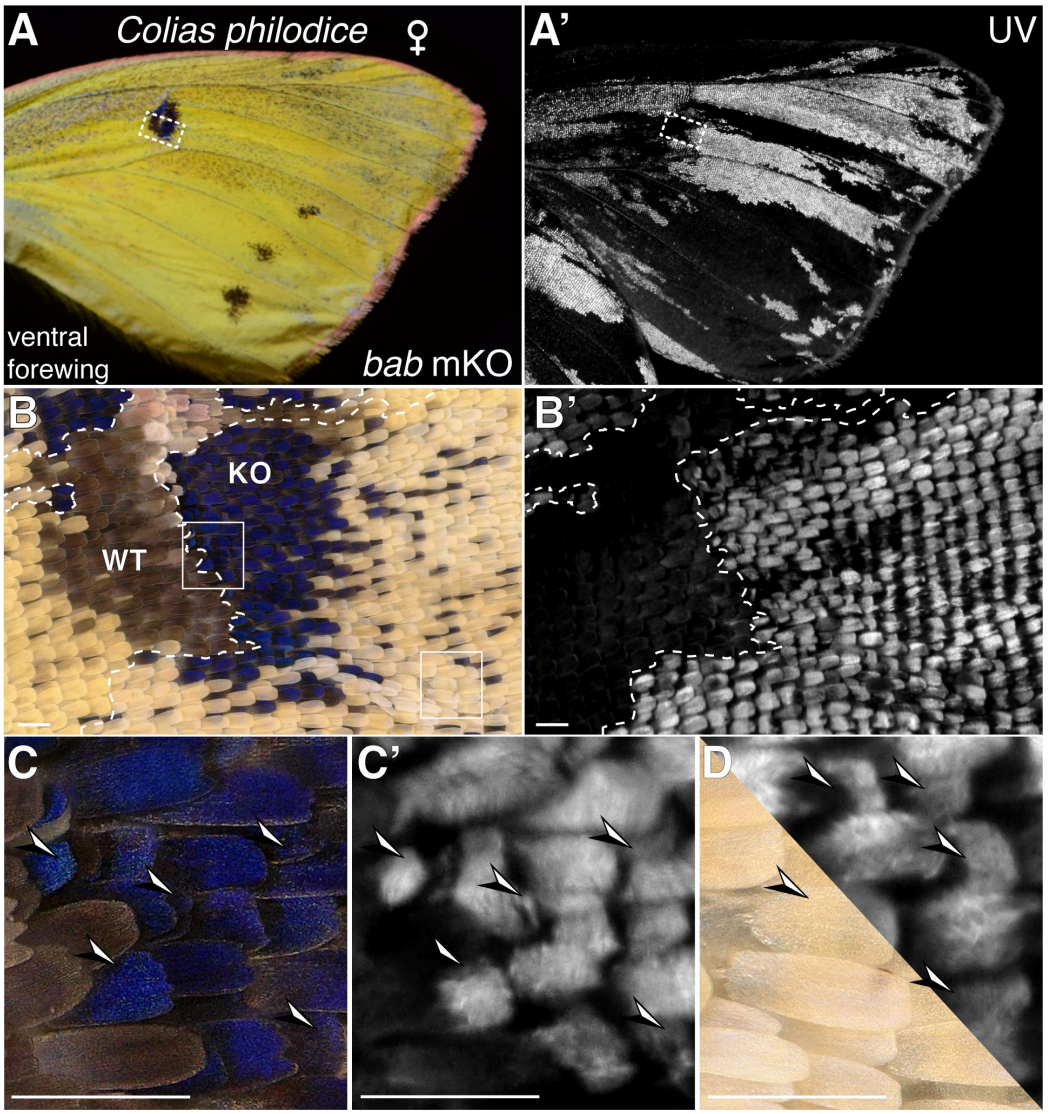

Figure S8. *bab* CRISPR mosaic KOs transform scales to the UV-iridescent state. (**A-B**) *bab* mKOs result in gain of UV-iridescence in both pterin and melanin pigment scales, here in the discal spot region of a female *C. philodice* ventral wing. (**C-D**) Magnified views from (**A-B**) showing the acquisition of UV-iridescence by mutant ground scales (arrowheads). Scale bars: 100 μm.

Figure S9. Female-specific effects of *bab* KO on pigmentation. (**A-B**) *C. eurytheme* females exhibit a gain of orange pigmentation in addition to UV transformation. When present, gain of orange is nested in UV transformed clones.

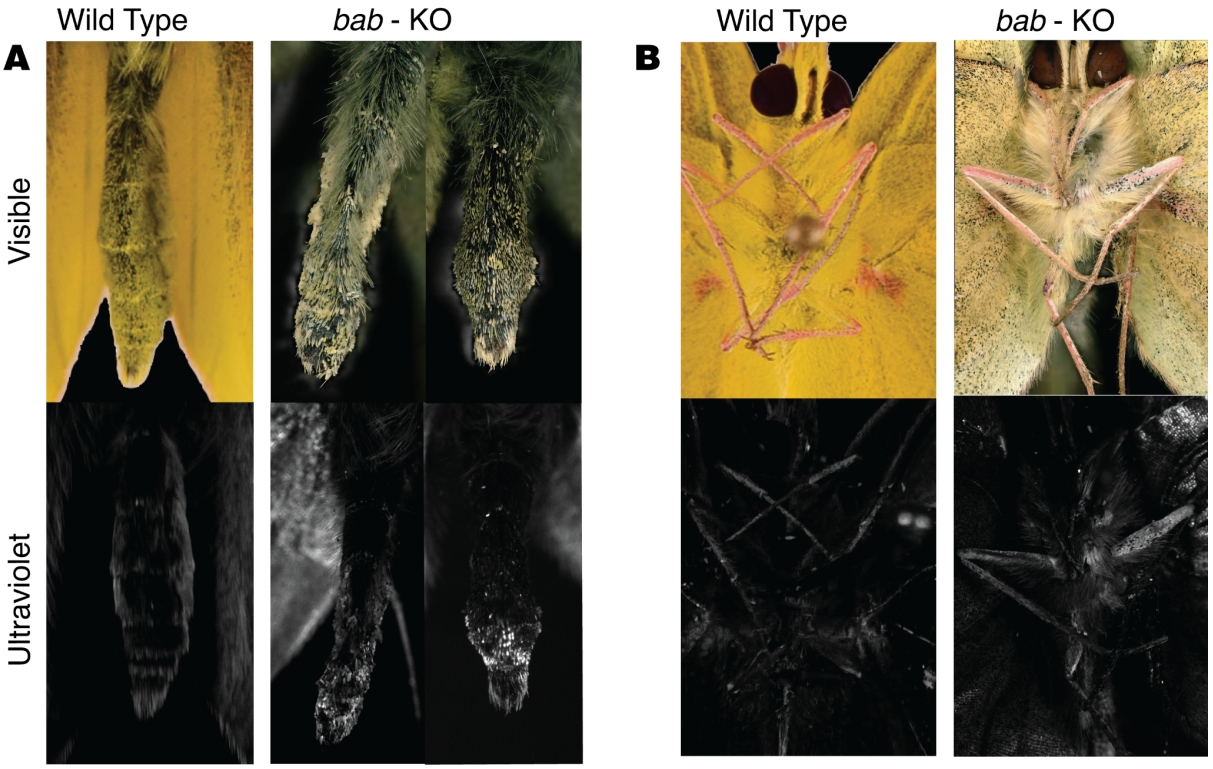

Figure S10. Gain of UV in abdominal and leg scales of *bab* G_0 crispants. (**A**) Abdominal and (**B**), leg scales of specimens exhibiting a gain of UV-iridescence in *C. eurytheme* male crispants. These body regions only display weak broad-spectrum reflectance in wild-type butterflies and do not iridesce in the UV.

Figure S11. CRISPR G_0 phenotypes following *bab* mosaic KO. First injection batch.

Figure S11 (*continued*). CRISPR G_0 phenotypes following *bab* mosaic KO.

Figure S11 (*continued*). CRISPR G_0 phenotypes following *bab* mosaic KO.

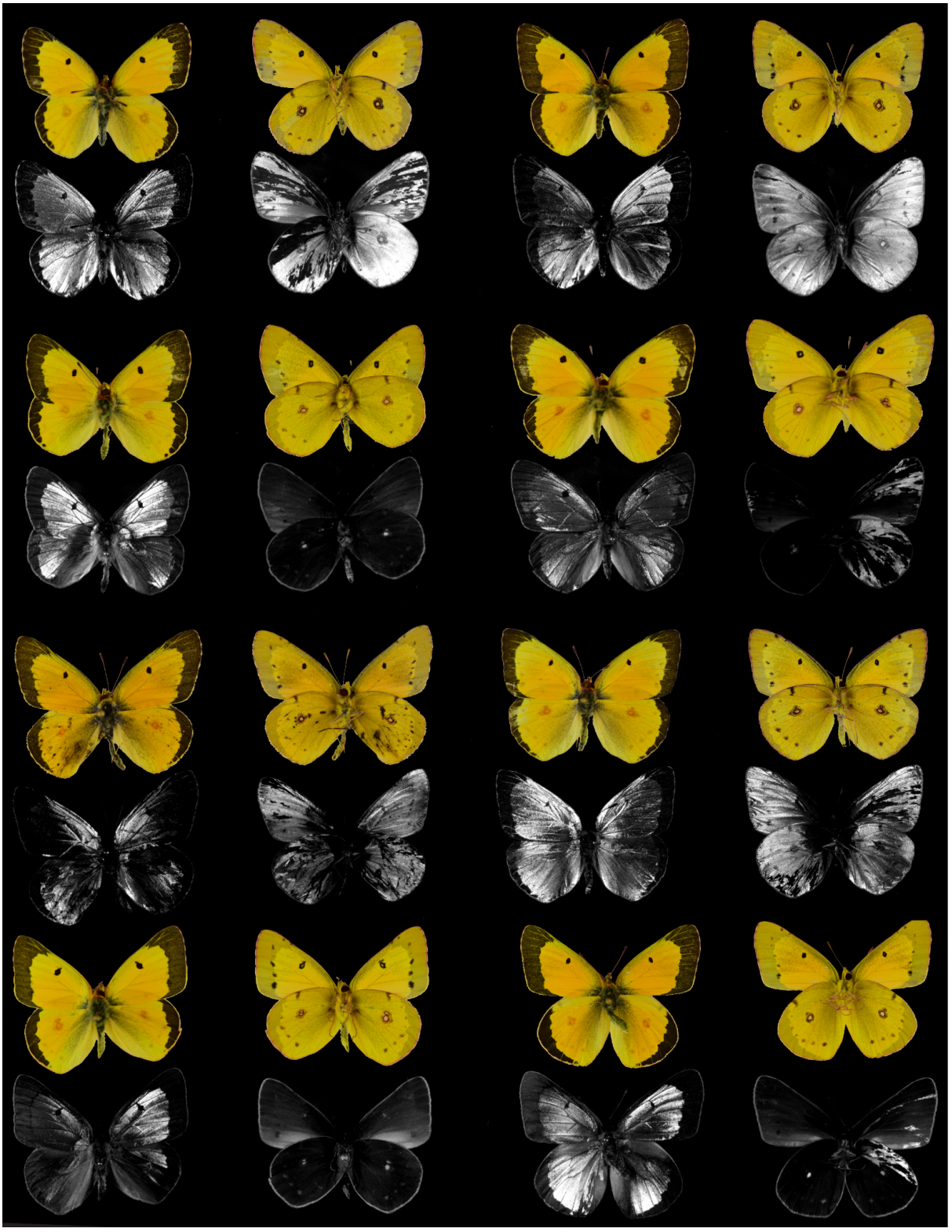

Figure S11 (*continued*). CRISPR G_0 phenotypes following *bab* mosaic KO.

Figure S11 (*continued*). CRISPR G_0 phenotypes following *bab* mosaic KO.

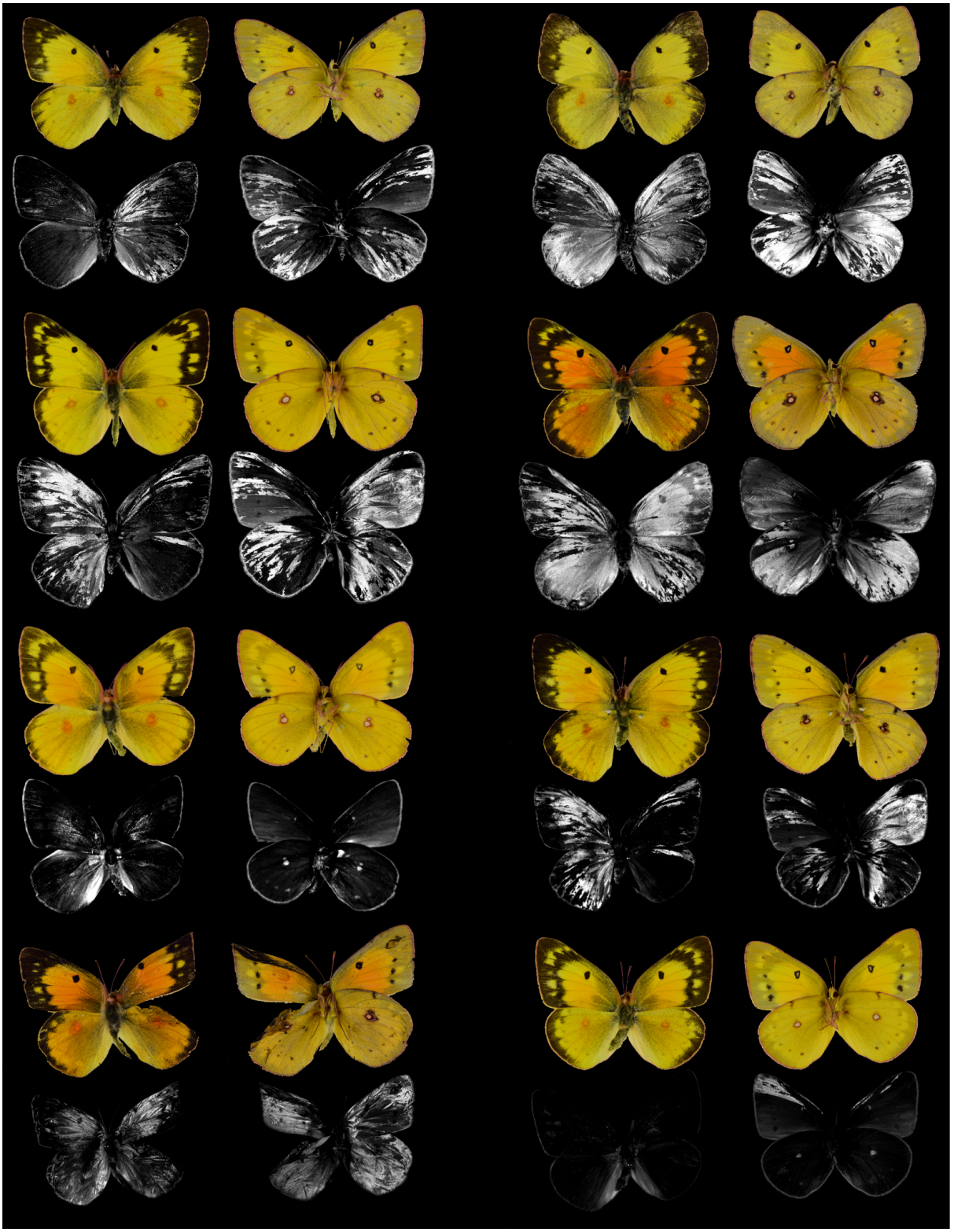

Figure S11 (*continued*). CRISPR G_0 phenotypes following *bab* mosaic KO.

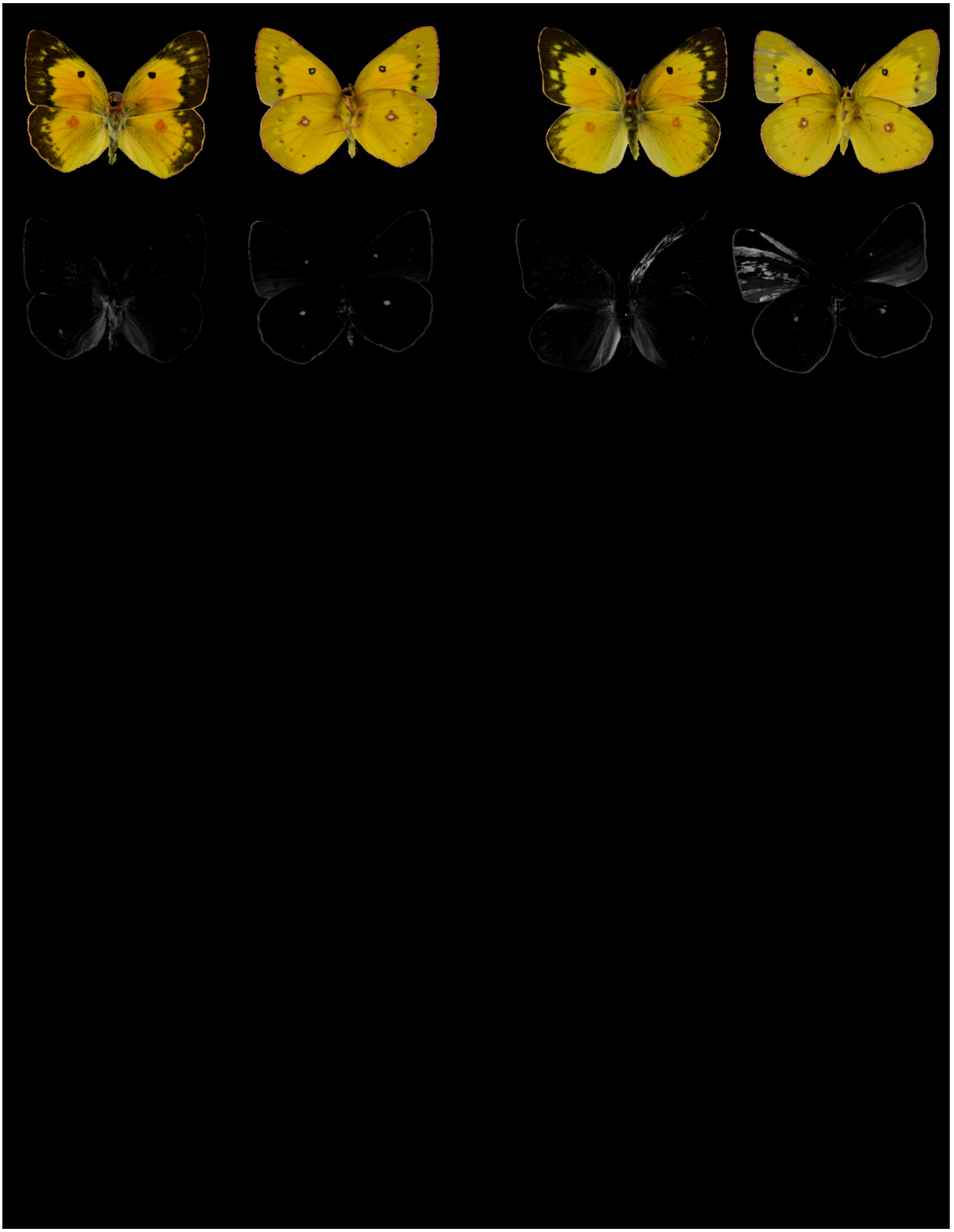

Figure S11 (*continued*). CRISPR G_0 phenotypes following *bab* mosaic KO.

Figure S12. CRISPR G_0 phenotypes following *bab* mosaic KO. Second injection batch.

Figure S12 (*continued*). CRISPR G_0 phenotypes following *bab* mosaic KO.

Supplementary Material Tables

Table S1. Resequenced samples for population genomics

Individual sample name	SRA Accession Number	Morphospecies	Color	UV trait	Sequencing coverage (x)	Notes
Ceu04	SRR12672378	*C. eurytheme*	Orange	UV+	14.3	Excluded from genome scan
Ceu16	SRR12672392	*C. eurytheme*	Orange	UV+	19.4	
Ceu17	SRR12672391	*C. eurytheme*	Orange	UV+	7.4	
Ceu18	SRR12672390	*C. eurytheme*	Orange	UV+	10.2	
Ceu21	SRR12672389	*C. eurytheme*	Orange	UV+	22.1	
Ceu23	SRR12672388	*C. eurytheme*	Orange	UV+	23.2	
Ceu24	SRR12672387	*C. eurytheme*	Orange	UV+	13.1	
Ceu26	SRR12672386	*C. eurytheme x philodice* hybrid	Orange	UV+	17.3	*C. eurytheme* PCA cluster, hybrid Z chromosome
Ceu27	SRR12672385	*C. eurytheme*	Orange	UV+	15.2	
Ceu29	SRR12672384	*C. eurytheme*	Orange	UV+	10.1	
Ceu30	SRR12672382	*C. eurytheme*	Orange	UV+	12.0	
Ceu31	SRR12672381	*C. eurytheme*	Orange	UV+	10.1	
Ceu32	SRR12672380	*C. eurytheme*	Orange	UV+	15.0	
Ceu35	SRR12672379	*C. eurytheme*	Orange	UV+	18.4	
Ceu_Miss	SRR14305386	*C. eurytheme*	Orange	NA	19.8	Sample from Mississippi
Cph01	SRR12672395	*C. philodice*	Yellow	UV-	18.0	
Cph02	SRR12672394	*C. philodice*	Yellow	UV-	13.0	
Cph03	SRR12672383	*C. philodice*	Yellow	UV-	8.2	Excluded from genome scan
Cph05	SRR12672377	*C. philodice*	Yellow	UV-	15.4	
Cph07	SRR12672376	*C. philodice*	Yellow	UV-	13.4	
Cph09	SRR12672375	*C. philodice*	Yellow	UV-	14.8	
Cph11	SRR12672374	*C. philodice*	Yellow	UV-	14.8	
Cph13	SRR12672373	*C. philodice*	Yellow	UV-	8.6	
Cph14	SRR12672372	*C. philodice*	Yellow	UV-	14.5	
Cph15	SRR12672393	*C. philodice*	Yellow	UV-	14.6	

Table S2. Summary statistics from the whole-genome population resequencing data

Statistic	d_{XY}	F_{ST}	$\pi_{philodice}$	$\pi_{eurytheme}$
Whole genome	0.146	0.042	0.130	0.136
Autosomes	0.143	0.027	0.133	0.137
Z-chromosome	0.205	0.337	0.071	0.103

Table S3. List of oligonucleotides used for 2b-RAD genotyping

Oligonucleotide name	Sequence (5'→3')	Notes
3illBC1	CAGACGTGTGCTCTTCCGATCT ACAC NG	Ligation 3' Adapters with 4-nt barcodes and NG (1/16th representation reduction)
3illBC2	CAGACGTGTGCTCTTCCGATCT GTCT NG	
3illBC3	CAGACGTGTGCTCTTCCGATCT TGGT NG	
3illBC4	CAGACGTGTGCTCTTCCGATCT CACT NG	
3illBC5	CAGACGTGTGCTCTTCCGATCT GATG NG	
3illBC6	CAGACGTGTGCTCTTCCGATCT TCAC NG	
3illBC7	CAGACGTGTGCTCTTCCGATCT CTGA NG	Original protocol by Mikhail Matz and Galina Aglyamova available at : https://github.com/z0on/2bRAD_denovo
3illBC8	CAGACGTGTGCTCTTCCGATCT AAGC NG	
3illBC9	CAGACGTGTGCTCTTCCGATCT GTAG NG	
3illBC10	CAGACGTGTGCTCTTCCGATCT GACA NG	
3illBC11	CAGACGTGTGCTCTTCCGATCT GTGA NG	
3illBC12	CAGACGTGTGCTCTTCCGATCT AGTC NG	
antiBC1	GTGTAGATCGGA/3InvdT/	For preparation of the Ligation 3' Adapter duplexes Terminated with 3' Inverted dT modification
antiBC2	AGACAGATCGGA/3InvdT/	
antiBC3	ACCAAGATCGGA/3InvdT/	
antiBC4	AGTGAGATCGGA/3InvdT/	
antiBC5	CATCAGATCGGA/3InvdT/	
antiBC6	GTGAAGATCGGA/3InvdT/	
antiBC7	TCAGAGATCGGA/3InvdT/	
antiBC8	GCTTAGATCGGA/3InvdT/	
antiBC9	CTACAGATCGGA/3InvdT/	
antiBC10	TGTCAGATCGGA/3InvdT/	
antiBC11	TCACAGATCGGA/3InvdT/	
antiBC12	GACTAGATCGGA/3InvdT/	
5ill-NG	CTACACGACGCTCTTCCGATCTNNRWCCNG	Ligation 5' Adapters with 4-nt barcodes and NG (1/16th representation reduction)
anti5ILL-NG	GGWYNNAGATCGG/3InvdT/	
NEBNext Universal primer	AATGATACGGCGACCACCGAGATCTACACTCTTTCC CTACACGACGCTCTTCCGATC*T	Universal TruSeq primer with phosphorothioate bond (*)
NEBNext Index 1-48 Primers for Illumina	CAAGCAGAAGACGGCATACGAGAT XXXXXX GTGACTGGAGTTCAGACGTGTGCTCTTCCGATCsT	Commercial NEBNext 6-nt barcoded primers
IC1-P5 ILL-Lib1	AATGATACGGCGACCACCGA	Standard Illumina library amplification primers
IC2-P7 (ILL-Lib2)	CAAGCAGAAGACGGCATACGA	

Table S4. Resequenced samples from the mapping broods

Brood and sample name	SRA Accession Number	Sex	UV trait	Sequencing coverage (x)	Notes
00-01-028	SRR14168767	f	UV-	16.7	*C. philodice*, paternal grandmother of 79
00-08-012	SRR14168766	f	UV-	19.9	*C. philodice*, maternal grandmother of 75
00-35-014	SRR14168748	m	UV-	16.4	F1, paternal uncle of 75, 49
00-43.5	SRR14168747	f	UV-	20.2	*C. eurytheme*, paternal grandmother of 75, 49
00-49-013	SRR14168746	m	UV+	16.2	Recombinant Z : 2b-RAD region 39-42 (Fig. S6)
00-49-016	SRR14168745	m	UV+	18.5	Recombinant Z (Fig. S6)
00-49-063	SRR14168743	m	UV-	17.5	Recombinant Z (Fig. S6)
00-49-086	SRR14168742	m	UV-	17.2	No recombinant Z
00-49-089	SRR14168765	m	UV+	20.5	Recombinant Z (Fig. S6)
00-49-182	SRR14168744	m	UV+	14.8	No recombinant Z
00-75-013	SRR14168764	m	UV+	22.8	No recombinant Z
00-75-022	SRR14168763	m	UV+	16.6	Recombinant Z : 2b-RAD region 39-42 (Fig. S6)
00-75-118	SRR14168762	m	UV+	16.6	Recombinant Z (Fig. S6)
00-75-138	SRR14168761	m	UV-	16.6	No recombinant Z
00-75-188	SRR14168760	m	UV+	25.6	No recombinant Z
00-79-013	SRR14168759	m	UV+	15.8	Recombinant Z : 2b-RAD region 39-42 (Fig. S6)
00-79-050	SRR14168758	m	UV+	17.1	Recombinant Z : 2b-RAD region 39-42 (Fig. S6)
00-79-055	SRR14168757	f	UV-	15.2	No recombinant Z
00-79-062	SRR14168756	m	UV+	17.0	No recombinant Z
00-79-073	SRR14168754	m	UV-	14.9	No recombinant Z
00-79-099	SRR14168749	m	UV+	18.3	Recombinant Z : 2b-RAD region 39-42 (Fig. S6)
00-79-108	SRR14168753	m	UV+	14.4	Recombinant Z (Fig. S6)
00-79-114	SRR14168752	m	UV+	25.4	Recombinant Z : 2b-RAD region 39-42 (Fig. S6)
00-79-119	SRR14168751	m	UV-	17.9	Recombinant Z (Fig. S6)
00-79-123	SRR14168750	m	UV+	26.0	No recombinant Z

Table S5. Annotated genes in the mapped *U* locus interval

***Colias eurytheme* v1 Assembly Gene ID**	**Flybase Orthologous Gene Name**	**Annotation Summary**
jg6723	*Knockout*	Axon guidance
jg6722	*l(1)G0289*	Plexin domain-containing
jg6721	*Drat*	Effector of ethanol induced apoptosis
jg6719 ; jg6720	*BtbVII*	BTB-POZ and Homeobox domain-containing transcription factor
jg6718	*Ptp61F*	Protein tyrosine phosphatase
jg6717	*ArfGAP1*	GTPase activating protein
jg6716	*Pex16*	Peroxisome organization, spermatocyte division, and fatty acid catabolism
jg6714	*CG9289*	Carboxylic ester hydrolase activity (predicted)
jg6715	*CG30283*	Serine-type endopeptidase activity (predicted)
jg6713	*CG42390*	GTPase activity (predicted)
jg6712	*sim*	Transcription factor, neural development, walking behaviour.
jg6709	*NimC4*	Phagocytosis of apoptotic cells
jg6701 ; jg6704	*ets65a*	Transcription factor
jg6703	*CG16789*	ATP-binding (predicted)
jg6702	*CG42526*	Transcription regulator (predicted)
jg6700	*Not1*	Poly-(A) ribonuclease, translation inhibition, ovarian follicle cell development
jg6699	*CNBP*	mRNA-binding, upregulates dMyc in developing wing
jg6695	***bab***	Transcriptional repressor with known roles in the suppression of male-specific features *(see main text)*